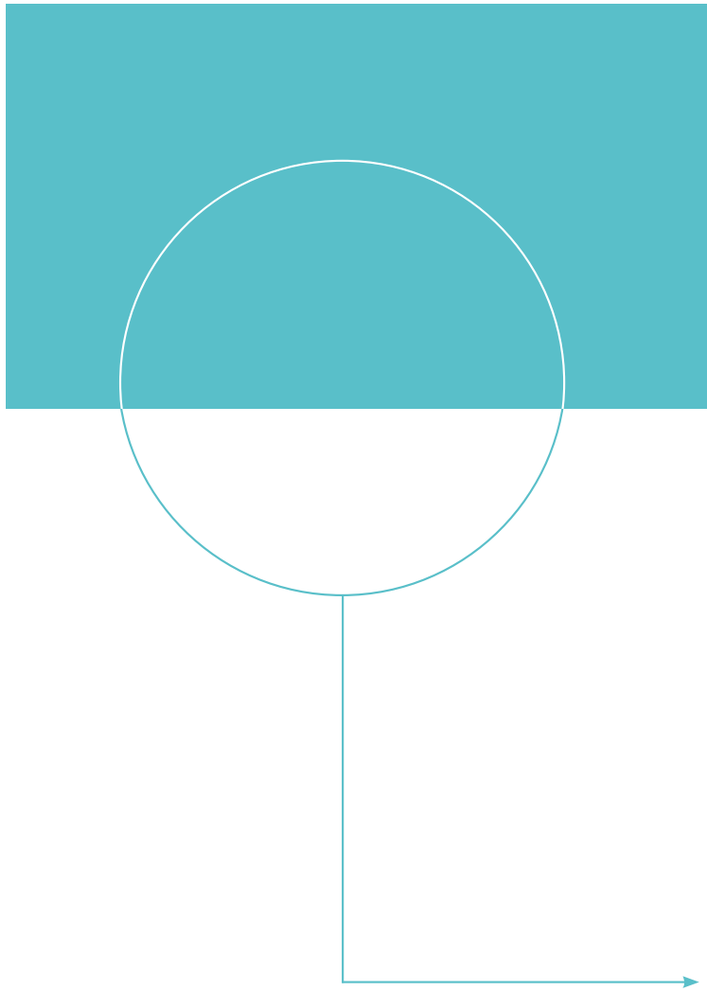

Master's thesis

2020

Oscar Ram Kalia

NTNU
Norwegian University of
Science and Technology
Faculty of Information Technology and Electrical
Engineering
Department of Engineering Cybernetics

Oscar Ram Kalia

Developing New Abilities for Humanoid Robots: How to Plan/Control a Sit-Down

June 2020

NTNU
Norwegian University of
Science and Technology

NTNU
Norwegian University of
Science and Technology

NTNU

Norwegian University of
Science and Technology

Developing New Abilities for Humanoid Robots: How to Plan/Control a Sit-Down

Oscar Ram Kalia

MTTK
Submission date: June 2020
Supervisor: Anton Shiriaev
Co-supervisor: Stepan Pchelkin

Norwegian University of Science and Technology
Department of Engineering Cybernetics

Abstract

This paper concerns biped humanoid robots and development of new abilites for these, especially performing a safe sit-down. Modelling, planning and analysis of this motion is addressed, by using a simplified model of a humanoid robot, namely the 3 *degree of freedom* (3DOF) model from [1] where knee and hip joints are actuated, while the ankle joint is assumed passive. Furthermore, an extension of said model is proposed, where a degree of freedom for actuated arms is added. The motion planning for this extended model is done, and some proposed control schemes are presented and discussed. Research on other papers relevant to the topic is done, and their methods in motion planning and results are compared with one another and with the work done in this paper. A biped humanoid robot performing a safe sit-down, and also a stand-up from sitting position, is seen to be feasible by emulating human behaviour. Whether human behaviour has to be replicated for planning a humanoid robot's movement is briefly discussed.

Contents

1 Introduction

There has been a lot of research on biped walking robots since the 1970s [5]. As technology has advanced, biped walking robots have evolved into biped humanoid robots. A *biped humanoid robot* is a robot which has two legs (*biped*), and an appearance resembling a human (*humanoid*). Furthermore, many researchers foresee that the humanoid robot industry will be one of the leading industries of the 21st century, and that humanity will eventually enter the age of having a functional robot in every home [6]. The interest for human-like robots dates back to 1920s science fiction. The term "robot" was first used in 1921 in a Czech play called Rossum's Universal Robots, by Karel Čapek. This play involves a factory that builds artificial people to be servants for humans, which are called robots [7]. The robots of our current day and age, especially humanoid ones, could to some extent be described as artificial people built to be servants for humans. At the same time, many people are skeptical of the technological advancements of robots and artificial intelligence (AI). They especially fear the dystopian future in which robots become so intelligent and self-aware they take over the world from the humans [8]. Either way, the technological development of robots will continue, regardless of what the future brings.

"Humanoid robots are electro-mechanical systems resembling the morphology of the human body. Consequently, it is very much desired to reproduce ordinary motions like humans." [9]

Development of new abilities for humanoid robots is of huge interest for the robotics community. The advancement is not happening at a very rapid pace, as this is a rather extensive field. For example, motion planning of a biped humanoid robot poses as a very challenging task, since a realistic humanoid robot will require many degrees of freedom (DOF) to accurately replicate a human. However, not all DOFs need to be actuated; a robot should only need to have an actuated state when it is of absolute necessity to perform a given task, to reduce system complexity. The result will be an underactuated system (see section 2.2), which has one or more passive degrees of freedom.

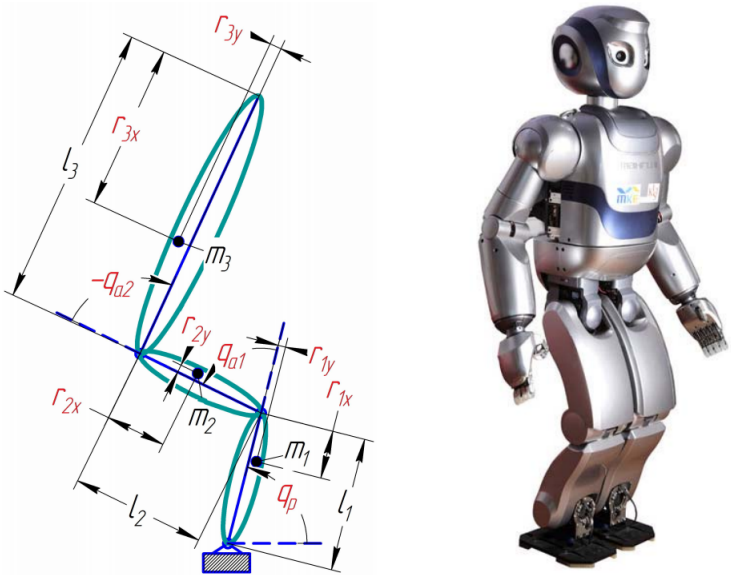

Figure 1: Left: Schematic of the planar 3DOF robot. Joint angles q_{a_1} for knee and q_{a_2} for hip are actuated, while ankle angle q_p is passive. Right: Humanoid robot *Mahru III*, courtesy of Samsung Electronics Co. [1]

This paper concerns biped humanoid robots and their ability to perform a safe sit-down from a standing position. All work presented in this paper is based on the model of a 3DOF planar robot (see Figure 1), as defined in [1]. This is an underactuated system, where the ankle joint is assumed passive. The concept of *virtual holonomic constraints* (VHC, see section 2.1) is used to help with

analysis and motion planning of the underactuated mechanical system presented. Moreover, a *motion generator* (MG, see section 2.4) for sit-down (or stand-up) trajectories to be generated by the robot is found.

One of the biggest motivations for developing new abilities for humanoid robots comes from the importance of such behaviours for rehabilitation and assistance for elderly and handicapped people, if they will be wearing robotic devices - e.g. *exoskeletons*. An *exoskeleton* is an external frame that can be worn to support the body, either to bypass physical limitations (become stronger or more agile) or to overcome the limitations of being injured or old [10]. An exoskeleton can assist an elderly person with doing day-to-day tasks such as walking, picking up things, sitting down and standing up, cooking, cleaning etc. Another application of this, which is arguably even more impressive, is that it can help paraplegics walk again.

An exoskeleton can be viewed as the outer skeleton of a biped humanoid robot (or at least a part of it), since it is supposed to fit on a human's body. This means that while the work done in this paper focuses on biped humanoid robots, the motion planning and analysis could be further applied to other robotic devices, such as exoskeletons.

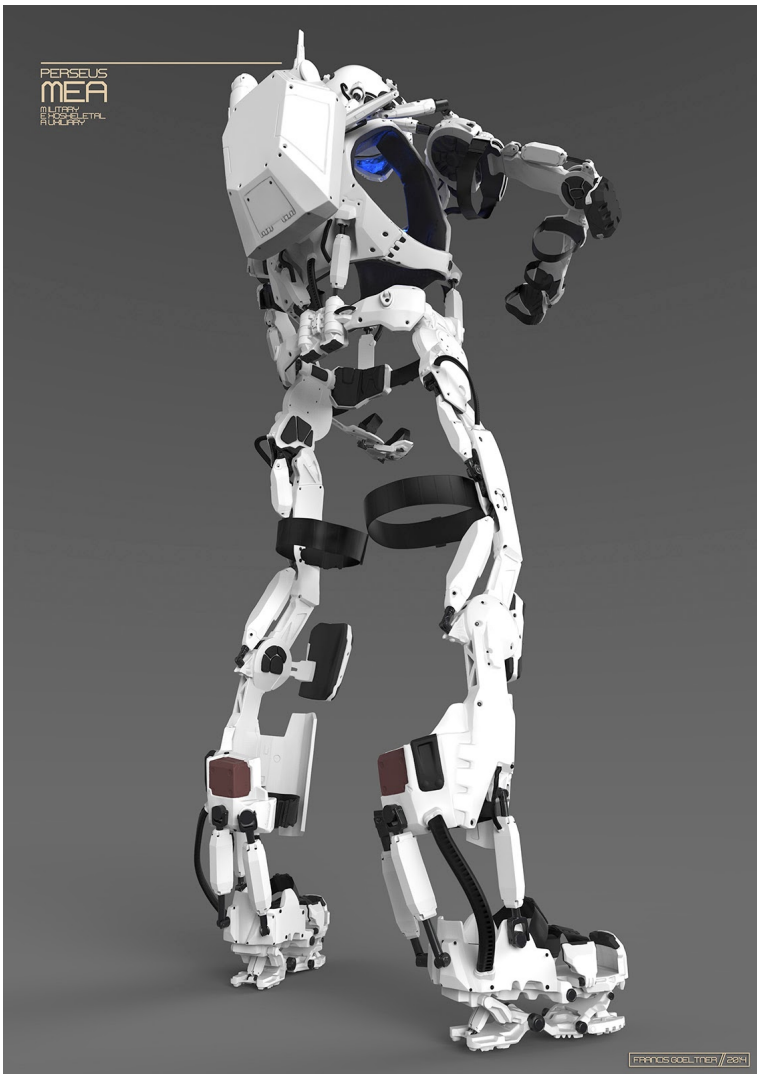

Figure 2: A concept for an exoskeleton, wearable by humans. [11]

"Humanoid robots shall not be restricted to follow only cyclic movement patterns such as walking or running; we might expect that they are capable of performing other motions as well. For example, they could sit down on a chair, pick up a book from the floor and put it on the shelf, handle

some tools, etc. In addition to autonomous humanoid robots which are mainly targeted at service robotics, there is also an interest in generating human-like motions for intelligent rehabilitation devices and prostheses. For example, a patient could train affected muscles by utilizing some kind of electro-mechanical attachment as well as an artificial leg with certain actuation." [9]

In this paper, motion planning and analysis for a biped humanoid robot's behaviour for sitting down is addressed. But what about standing up? Will a stand-up from sitting position be the exact same procedure as sitting down, but in reverse? Is this the case for humans? Also, will a humanoid robot have to replicate a human's behaviour to safely sit-down, or can it have some unhumanlike configurations? One would think this would be possible, but for exoskeletons one has to be careful when implementing this. It should not be of any issue for a humanoid robot to act in some unhuman-like behaviour, if this makes a given task easier. An example of this is when the robot moves or rotates its limbs in a way a human couldn't physically do without injury. However, when addressing wearable robotic devices, such as exoskeletons, it could have fatal consequences for the human if the robot were to twist and turn in unhuman-like manners.

A humanoid robot will have to face uncertainties in environment, such as uneven terrain, which leads to nonlinear dynamics. If each degree of freedom is equipped with an actuator, it might be inefficient and unnaturally looking. For underactuated systems, one can apply developed tools for periodic gait synthesis and orbital stabilization. A human (humanoid robot) cannot apply large values of control torque at the ankle joint, since muscles (actuator) at this joint is not powerful enough to rotate the whole body. Therefore the ankle joint is assumed to be completely passive, and the result is an underactuated system [1].

With tools for handling underactuated systems, such as virtual holonomic constraints (VHC, see section 2.1), motion planning and analysis for the 3DOF planar robot (Figure 1) can be done, as seen in [1]. Moreover, one could extend this model to work for additional degrees of freedom. In this paper, an extended model with an added degree of freedom for actuated arms is proposed. Furthermore, motion planning and analysis of this extended 4DOF model is done, and a few control schemes aimed at controlling the robot's sit-down behaviour are presented and discussed. In addition, a few other papers on similar topics are presented, discussed, and compared with the work done in this paper.

2 Theory

This section covers definitions and theory of different concepts that are mentioned throughout the paper. All work presented in this paper is based on the 3DOF planar robot, with parameters from the humanoid robot *Mahru III* [12], as seen in Figure 1. This system is an *underactuated* (mechanical) system, and the term is defined in this section (2.2). Recent developments in nonlinear control theory is used, namely the method of *virtual holonomic constraints* (2.1). This allows for exponential *orbital stabilization* (2.3) of periodic motions of underactuated systems. This approach lets us derive a scalar *motion generator* (MG, 2.4) equation for systems with a degree of underactuation equal to one, which the planar 3DOF robot is. The MG can be used as a central pattern generator. The technique is further extended to deal with motions of finite time intervals, which is useful since a sit-down is a short-lasting movement. [1]

2.1 Virtual Holonomic Constraints (VHC)

The notion of virtual holonomic constraints (VHC) serves as a very useful tool for motion planning, control and analysis of mechanical systems. VHCs are used to reduce a motion planning problem to search for an acceptable timing function in the phase plane of the geometric path coordinate. Some systems are fully actuated (e.g. industrial manipulators), and any timing along the path can be achieved as long as the corresponding differential constraints - accelerations and velocities - are not violated. The same cannot be said for *underactuated mechanical systems* (definition given in section 2.2).

The concept of virtual constraints is rather new in the field of nonlinear feedback control. It serves as a tool for orbitally stabilizing underactuated mechanical systems. Geometric functions among generalized coordinates show up during a feasible motion, rather than actual physical motion, which are called virtual holonomic constraints [13]. The concept is properly explained in the definition below.

Definition 1 - Virtual Holonomic Constraints [14]
Given the motion of a controlled Euler-Lagrange system with n degrees of freedom

$$M(q)\ddot{q} + C(q,\dot{q})\dot{q} + G(q) = B(q)u \tag{1}$$

and the set of geometric relations among the generalized coordinates given by

$$\Big\{q_1 = \phi_1(\theta),\ \ q_2 = \phi_2(\theta),\ \ \ldots,\ \ q_n = \phi_n(\theta)\Big\}, \quad \theta = \theta_\star(t), \quad t \in [0,T], \tag{2}$$

the motion (1) can be represented by (2) as a vector function

$$q = \Phi(\theta) \tag{3}$$

and a scalar time-parameterizing variable θ. The equation $q = \Phi(\theta)$ is called a

- *holonomic (geometric) constraint if it represents a restriction on generalized coordinates physically imposed on the system;*
- *virtual holonomic (geometric) constraint if the relation is preserved by some control action along solutions of the closed-loop system, provided that initial conditions are chosen to satisfy the constraint: $q(0) = \Phi(\theta(0))$ and $\dot{q}(0) = \Phi'(\theta(0))\dot{\theta}(0)$.*

Holonomic constraints represent a restriction in the configuration space of the mechanical system to one specific curve.

2.2 Underactuation

An underactuated mechanical system is a system which has fewer independent control inputs than generalized coordinates. An underactuated system has one or more passive degrees of freedom.

Definition 2 - Underactuation
Given the motion of a controlled Euler-Lagrange system (1), with $n = dim(q)$ degrees of freedom and $m = dim(u)$ control inputs, the system is called ***underactuated*** *if the following holds;*

$$0 \leq m < n,$$

i.e. if the number of control inputs is less than the amount of degrees of freedom.

2.3 Orbital Stability

The concept of orbital stability is important when talking about trajectories of underactuated systems. One definition is given below.

Definition 3 - Orbital stability [15]
Given the ordinary differential equation

$$\dot{x} = f(x),$$

we say that $x(t)$ is an ***orbitally stable solution*** *if $\forall \varepsilon > 0$, $\exists \delta > 0$ such that for any solution $y(t)$ with $||x(t_0) - y(t_0)|| < \delta$ it holds that for all $t > t_0$ there exists some $s > t_0$ so that $||x(s) - y(t)|| < \varepsilon$.*

2.4 Motion Generator

A *motion generator* is a dynamical system of low dimension whose solutions define the evolution of all degrees of freedom of a higher-dimensional mechanical system. Given the motion of a controlled Euler-Lagrange system with n degrees of freedom (1), where one of the degrees of freedom is assumed passive, one can start searching for a solution of this system of underactuation one by describing the actuated limbs evolutions q_{a_j} as a function of the passive DOF q_p,

$$q_{a_j} = \sum_{i=0}^{m} k_{ij} q_p^i, \qquad 1 \leq j \leq n-1, \qquad m \in [1, n]. \tag{4}$$

Note that this choice is not fixed a priori, but a sufficient choice has to be found to reflect the particular motion in question. This particular choice was found to be sufficient for reflecting the sit-down of a planar robot model. The parameter m denotes the degree of the polynomial, and is chosen to be somewhere between 1 and n for this system. Substituting the equations q_{a_j} and their first and second time derivatives into the dynamics of the passive degree of freedom q_p in (1) and collecting terms, we obtain the second order differential equation

$$\alpha(k_{ij}, q_p)\ddot{q}_p + \beta(k_{ij}, q_p)\dot{q}_p^2 + \gamma(k_{ij}, q_p) = 0. \tag{5}$$

The α, β, γ-equation (5) can be used as a motion generator for the system. For this particular system, it serves as a MG for sit-down (or stand-up) trajectories to be generated for the robot. By finding the right k_{ij}, and an appropriate time evolution of q_p is found as a solution of (5), then the corresponding behaviours for the actuated joints q_{a_j} are determined by (4). However, note that the coefficients of the MG are dependent on the unknown parameters k_{ij}. These are to be found by optimization, such that the MG inherits certain qualitative and quantitative features decided by some initial data. By optimizing after certain configuration, velocity and actuation constraints, as well as knowing what features are desired for the particular motion, the coefficients k_{ij} can be found, which completes the MG. [1]

3 Methodology

The work done in this paper is based on the model presented by Stepan Pchelkin et.al. in [1], see Figure 1. The model is a simplified model of a biped humanoid robot, with the purpose of motion planning, analysis and control of sit-down behaviour. The method and steps in motion planning is covered in Section 3.1. Note that the motion planning of the 3DOF model covered in Section 3.1 is a repetition of what has already been done in [1]. A proposal for an extension of the model is covered in section 3.2. The extension proposed is the 4DOF planar robot model with an added degree of freedom for actuated arms.

Morover, research on other similar projects involving biped humanoid robots and their ability to sit-down (or stand up) was done, by searching the internet. See section 3.3 for the motion planning procedures from these papers.

3.1 3 Degree of Freedom (3DOF) Model

The human body has a very complex structure, and trying to model every degree of freedom is regarded as infeasible. On the other hand, when a specific motion is regarded, a reasonably simplified model can be applied. For sitting down and rising from a sit-down position, a model of the human body can be simplified into three links, as seen in Figure 1. The 3DOF model is used to describe a sit-down behaviour for a humanoid, which is considered reasonable as it is compared to recorded human behaviour, as seen in [16].

Parameter	Lower Leg	Upper Leg	Upper Body
Length [m]	$l_1 = 0.29$	$l_2 = 0.29$	$l_3 = 0.6115$
Mass [kg]	$m_1 = 6.986$	$m_2 = 6.746$	$m_3 = 41.739$
Distance to CoM_x [m]	$r_{1x} = 0.08252$	$r_{2x} = 0.1421$	$r_{3x} = 0.3544$
Distance to CoM_y [m]	$r_{1y} = -0.0066$	$r_{2y} = -0.02228$	$r_{3y} = 0.01408$
Inertia about CoM [kg·m^2]	$J_{c1} = 0.06618$	$J_{c2} = 0.06391$	$J_{c3} = 1.06165$
Gravitational constant		$g = 9.81$ m/s^2	

Table 1: Parameters of the planar 3DOF pendulum (see Figure 1) that represents a non-trivial part of the robot dynamics for 28 DOFs of the humanoid robot *Mahru III* [12] along the sit-down behaviour. [1]

In order to plan the motion of a safe sitting down for a realistic example, the parameters of the humanoid robot *Mahru III*, built at the Mechatronics & Manufacturing Technology Center of Samsung Electronics Co. [12], were used. The parameters are given in Table 1. The robot has 28 DOFs, and the Euler-Lagrange equations describing its dynamics are

$$M(q)\ddot{q} + C(q,\dot{q})\dot{q} + G(q) = B(q)u, \qquad q \in \mathbb{R}^{28}. \tag{6}$$

Here u is a vector of external generalised forces and $B(\cdot)$ is a coupling-matrix function defined by the location of the controlled generalised forces. $M(\cdot)$, $C(\cdot)$ and $G(\cdot)$ are derived from kinetic and potential energies of the control-free mechanism. Furthermore, we assume that only 3 DOFs are experiencing substantial changes, while the remaining 25 DOFs are assumed to be unvarying;

$$q_i(t) \equiv q_i(0), \qquad i = 4, \ldots, 28. \tag{7}$$

The remaining 3DOF dynamics boils down to an equivalent of a 3-link planar pendulum, as seen in Figure 1. We can write the dynamics as

$$M_3(q)\begin{bmatrix}\ddot{q}_p\\ \ddot{q}_{a1}\\ \ddot{q}_{a2}\end{bmatrix} + C_3(q,\dot{q})\begin{bmatrix}\dot{q}_p\\ \dot{q}_{a1}\\ \dot{q}_{a2}\end{bmatrix} + G_3(q) = \begin{bmatrix}0\\ \tau_{a1}\\ \tau_{a2}\end{bmatrix}, \tag{8}$$

where q_p is the angle of the passive ankle joint, q_{a1} is the angle of the actuated knee joint and q_{a2} is the angle of the actuated hip joint. In addition, τ_{a1} and τ_{a2} are control torques applied at the knee and hip joints respectively. $M_3(q)$ is the inertia matrix, $C_3(q,\dot{q})$ is a matrix corresponding to the Coriolis and centrifugal generalised forces and the vector $G_3(q)$ accounts for gravity.

3.1.1 Motion Planning: Motion Generator

By using the results from the analysis of a recorded human motion reported in [16], we can start searching for a solution of (8), by describing the actuated limbs evolutions q_{a1} (knee) and q_{a1} (hip) as a function fo the passive DOF q_p,

$$q_{a1} = k_{01} + k_{11}q_p + k_{21}q_p^2 + k_{31}q_p^3 \tag{9}$$

$$q_{a2} = k_{02} + k_{12}q_p + k_{22}q_p^2 + k_{32}q_p^3. \tag{10}$$

The choice is not fixed a priori, but a sufficient choice is found to reflect the particular motion in question. By substituting the relations (9)-(10) and their first and second time derivatives into the dynamics of the passive degree of freedom q_p in (8) and collecting terms, we obtain the second order differential equation

$$\alpha(k_{ij}, q_p)\ddot{q}_p + \beta(k_{ij}, q_p)\dot{q}_p^2 + \gamma(k_{ij}, q_p) = 0, \tag{11}$$

which serves as a motion generator (MG, see section 2.4) for sit-down trajectories to be generated for the robot. The values of k_{ij} are to be found by optimization for finding a human-like motion, which is covered in section 3.1.2.

3.1.2 Motion Planning: Human-Like Motion via Optimization

Coefficients of the MG (11) are dependent on the unknown parameters k_{ij} in (9)-(10). These are to be searched for such that the MG (11) inherits certain qualitative and quantitative features of such a dynamical system found when analysing recorded human behaviours. Referring to a paper which recorded human motions, [16], the following desirable features of the motion are found:

I The angular velocity $\dot{q}_p^h(t)$ of the ankle joint is small both in the beginning and at the end.

II The angular acceleration $\ddot{q}_p^h(t)$ is small at the end.

III All the equilibrium points q_{pe} of the MG (11) are outside the range of the ankle angle [min q_p^h, max q_p^h].

IV The finite-time evolution of $q_p^h(\cdot)$ along a sitting-down motion is part of a cycle of its MG (11).

The desirable features I-IV are the qualitative characteristics of the motion. In addition, a sit-down motion of the robot should comply with the following velocity, actuation and configuration constraints:

i The ankle angle q_p is expected to decrease monotonically from 1.5 to 1 [rad].

ii The knee angle q_{a1} is expected to grow monotonically from 0.4 to 1.6 [rad].

iii The hip angle q_{a2} is expected to decrease monotonically from -0.4 to -1.6 [rad].

iv The external torque in the ankle joint along the motion should be zero.

v The external torque of the knee joint is limited to $\pm$ 75 [Nm].

vi The external torque of the hip joint is limited to $\pm$ 80 [Nm].

vii The execution time to complete the motion is $\approx$ 0.5 [s].

This list is not final, and could be extended to include e.g. desired initial and final configurations of the robot, velocities and accelerations required at the end of the motion, actuator constraints, constraints on normal force acting on the feet etc.

To start looking for a human-like motion via a constrained optimization, we first need to choose a performance index. The index should either reflect critical features of the desired motions of the robot, or critical constraints that the motions must account for - e.g. in actuation. We suggest to

search for the parameters k_{ij} that shape the phase portrait of the robot MG (11) and comply with the features of human motion I-IV through minimization of the index

$$W(k_{ij}) = \int_{\tau}^{T_R} |\dot{q}_p(t)|^2 dt + \lambda \cdot (T_R - T_H)^2, \tag{12}$$

where $T_H \approx 0.5$ [s] is the time required for a human to sit down, T_R is the time the robot uses for the motion, τ is a constant which decides the size of the time interval (τ, T_R), where $\dot{q}_p(\cdot)$ is expected to remain small, and $\lambda > 0$ is a weight. Furthermore, the integral part of the index (12) accounts for motions that meet the specifications I and II from the list of features observed for the human MG (11). The remaining part of the index takes the total time of the motion into account, and penalises if it is not sufficiently close to the human motion. Meanwhile, the features III and IV yield a mathematical characterisation in terms of unknown parameters k_{ij} of (9)-(10), which can be rewritten as constraints for the parameters k_{ij}. The following statements are the conditions for III and IV, respectively.

Statement 1 - Conditions for Feature III
The system (11) has no equilibrium on the interval $q_p \in [q_p^{min}, q_p^{max}]$ if the following holds;

$$\gamma(k_{ij}, q_p) \neq, \qquad \alpha(k_{ij}, q_p) \neq \infty, \qquad \forall q_p \in [q_p^{min}, q_p^{max}].$$

Statement 2 - Conditions for Feature IV
Suppose the coefficients of (11) are smooth and the system has no equilibrium on $[q_p^{min}, q_p^{max}]$. Let q_e be an equilibrium of the system (11), i.e. a point where $\gamma(k_{ij}, q_e) = 0$, such that the following statements are true;

A) *$q_e < q_p^{min}$ and this is the first equilibrium below q_p^{max}, i.e. $\gamma(k_{ij}, q_e) \neq 0$ and $\alpha(k_{ij}, q_p) \neq \infty, \forall q_p \in (q_e, q_p^{min}]$,*

B) *the equilibrium q_e is to make sure the following inequality holds*

$$\left.\frac{\gamma'(k_{ij}, q_p)}{\alpha(k_{ij}, q_p)}\right|_{q_p = q_e} > 0.$$

Then, there exists $\varepsilon > 0$ such that any solution of the system (11) with initial conditions

$$q_p(0) \in [q_p^{min}, q_p^{max}], \qquad \dot{q}_p(0) \in [-\varepsilon, \varepsilon],$$

is a limit cycle of (11), encircling the equilibrium $q_p = q_e$.

3.1.3 Virtual Holonomic Constraints of the Model

The structure of the virtual holonomic constraints (for definition, see section 2.1) is chosen as a polynomial of order 3. The VHCs for the 3DOF model are

$$\phi_1 = 0 \tag{13}$$
$$\phi_2 = k_{24} - [k_{23}\theta_0^3 + k_{22}\theta_0^2 + k_{21}\theta_0] \tag{14}$$
$$\phi_3 = k_{34} - [k_{33}\theta_0^3 + k_{32}\theta_0^2 + k_{31}\theta_0], \tag{15}$$

where

$$\theta_0 = \frac{\pi}{2} - 1.45$$

is the initial condition for ankle angle. The VHCs correspond with the degrees of freedom for the model; ϕ_1 is for the passive ankle angle, ϕ_2 is for the actuated knee joint angle and ϕ_3 is for the actuated hip joint angle. The coefficients k_{ij} are to be found by the same optimization procedure as the one covered in 3.1.2.

3.2 Extension of the Model - 4DOF Model with Actuated Arms

As an extension of the already established 3DOF model as seen in Figure 1, the 4DOF model with an added *degree of freedom for actuated arms* is considered in this section, assuming both arms move identically in the sagittal plane. The dynamics of the 4DOF model can be written as

$$M_4(q)\begin{bmatrix}\ddot{q}_p\\ \ddot{q}_{a1}\\ \ddot{q}_{a2}\\ \ddot{q}_{a3}\end{bmatrix} + C_4(q,\dot{q})\begin{bmatrix}\dot{q}_p\\ \dot{q}_{a1}\\ \dot{q}_{a2}\\ \dot{q}_{a3}\end{bmatrix} + G_4(q) = \begin{bmatrix}0\\ \tau_{a1}\\ \tau_{a2}\\ \tau_{a3}\end{bmatrix}, \tag{16}$$

where q_{a3} is the angle of the actuated arms. Furthermore, we can parametrize q_{a3} as a polynomial of q_p, to get

$$q_{a3} = k_{03} + k_{13}q_p + k_{23}q_p^2 + k_{33}q_p^3. \tag{17}$$

3.2.1 Motion Planning: Motion Generator

Substituting the expression for q_{a3} from (17) together with the expressions for q_{a1} and q_{a2} from (9)-(10) into the passive dynamics of (16), we get a new motion generator for the 4DOF system;

$$\alpha_4(q_p)\ddot{q}_p + \beta_4(q_p)\dot{q}_p^2 + \gamma_4(q_p) = 0. \tag{18}$$

The coefficients $\alpha_4(q_p)$, $\beta_4(q_p)$ and $\gamma_4(qp)$ of the new motion generator (18) now depend on twelve parameters k_{ij} to be tuned, instead of eight as it was for (11). The coefficients are to be found by optimizing a performance index subject to the list of previous constraints, as well as additional requirements for the motion of arms. This procedure is covered in section 3.2.2.

3.2.2 Motion Planning: Optimization

To start searching for the coefficients of (18) via optimization, an objective function and some constraints have to be defined. In this case, we suggest to minimize the values of control torques for the actuated joints, namely knee, hip and arms. Naming the objective function F, we have the following objective to minimize:

$$F = \tau_{a1}^2 + \tau_{a2}^2 + \tau_{a3}^2,$$

where all constraints from section 3.1.2 are active. In addition, we need some new constraints for the arm motion. Since we do not expect the arms move much during a sit-down motion, especially in this case where each arm stays completely straight throughout the motion (hence only one degree of freedom for the arms), we suggest to keep the angle of the arms within a reasonably small range. Additionally, we expect the torque to stay within a reasonable range as well. A suggestion for new constraints:

1 The angle of the arms q_{a3} should not exceed ± 0.5 [rad].

2 The external torque of the arm joint is limited to ± 50 [Nm].

Please note that the values in constraints 1-2 are taken from pure speculation, and not from recorded human motions like the constraints i-vii from section 3.1.2 are.

3.2.3 Virtual Holonomic Constraints of the Extended Model

By adding another degree of freedom to the model, an additional virtual holonomic constraint has to be included. The VHC will still be a polynomial of degree 3, and will take the form

$$\phi_4 = k_{44} - [k_{43}\theta_0^3 + k_{42}\theta_0^2 + k_{41}\theta_0], \tag{19}$$

where VHCs (13)-(15) are active, and

$$\theta_0 = \frac{\pi}{2} - 1.45$$

is the initial condition for ankle angle. The coefficients k_{ij} are to be found by the same optimization procedure as the one covered in section 3.2.2.

3.3 Other Papers on the Topic

In this section a few other papers and their methods in motion planning for humanoid robot sit-down/stand-up are briefly presented. For results from these motion planning procedures, see section 4.3. For further discussion on these results, and comparison with the work done in this paper, see section 5.4.

3.3.1 Sit-to-Stand Task on a Humanoid Robot from Human Demonstration [2]

In [2], the task was to make a (biped) humanoid robot stand up from a sit-down position. The robot used is the Carnegie Mellon/Sarcos hydraulic humanoid robot (see Figure 3), and finding centers of mass (CoM) for this robot is non-trivial, since electronics, hydraulic hoses and onboard computers have to be accounted for. The proposed procedure for finding this is to track a human demonstrator's CoM trajectory as closely as possible, to realize natural human motion.

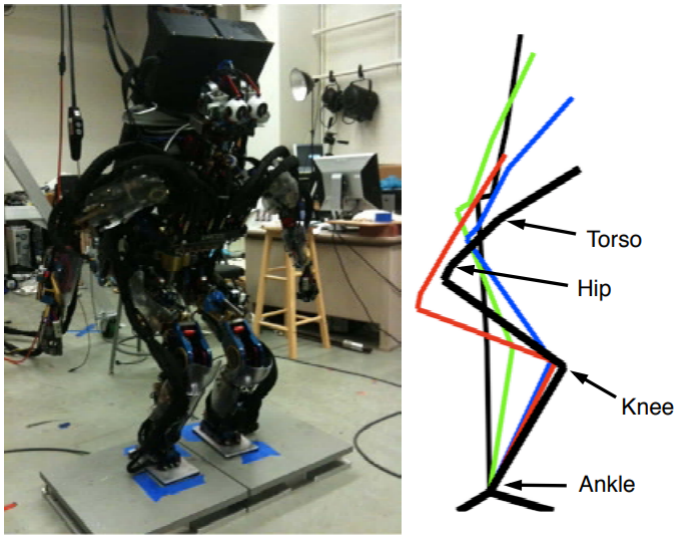

Figure 3: Left: The Carnegie Mellon/Sarcos humanoid robot standing in a squat position. Right: Some sample postures for data collection.

To obtain a more accurate estimate of the robot's CoM position, a simplified version of a least-squares optimization inertial parameter identification is used. The model presented is of a floating base rigid body robot, and its dynamics is given by

$$K(q, \dot{q}, \ddot{q})\phi = S^T\tau + J_C^T(q)\lambda, \tag{20}$$

where $q \in \mathbb{R}^{n+6}$ is the configuration vector for the robot (6 DOF floating base and n joints), $\tau \in \mathbb{R}^n$ is the vector of torques for actuated DOFs, $S = [0_{n\times 6} \;\; I_{n\times n}]$ delineates actuated and unactuated DOFs (the floating base is unactuated), J_C is the contact Jacobian matrix and λ is the vector for contact forces. The vector $\phi = [\phi_0^T \;\; \dots \;\; \phi_n^T]^T$ is of inertial parameters of n links for joints plus 1 floating base link, and each link has 12 parameters;

$$\phi_i = [m_i \;\; m_i c_{x_i} \;\; m_i c_{y_i} \;\; m_i c_{z_i} \;\; I_{xx_i} \;\; I_{xy_i} \;\; I_{xz_i} \;\; I_{yy_i} \;\; I_{yz_i} \;\; I_{zz_i} \;\; f_{c_i} \;\; f_{v_i}]^T, \tag{21}$$

where m_i is the mass of link i, the c_{a_i} components are the link's center of mass position, and the I_{ab_i} components are the independent components of its inertia tensor. In addition, f_{c_i} is the coloumb friction, and f_{v_i} is the viscous friction.

Furthermore, the dynamics are further simplified, by only regarding static postures of the robot. The reduced dynamics is then given by

$$K_g(q)\phi_g = S^T\tau + J_C^T(q)\lambda, \tag{22}$$

where

$$\phi_{g,i} = [m_i \quad m_i c_{x_i} m_i c_{y_i} m_i c_{z_i}]^T. \tag{23}$$

By denoting the vector f for total generalized force as

$$f_i = S^T \tau_i + J_{C_i}^T \lambda_i \tag{24}$$

for each $K_g(q_i)$ for a static posture given by q_i, the estimate of inertial parameters can be found by using ordinary weighted least squares:

$$\hat{\phi}_g = (\bar{K}_g^T \bar{K}_g)^{-1} \bar{K}_g^T \bar{f}, \tag{25}$$

where the bar notation refers to a stack of matrices for several static postures, which will compute the parameter set $\hat{\phi}_g$ that minimizes $||\bar{K}_g \hat{\phi}_g - \bar{f}||_2$. Moreover, the motion generation is to be found by measuring a human actor's CoM while imitating an elderly persons stand-up motion.

3.3.2 Sit-to-Stand Motion Analysis for NAO Humanoid Robot [3]

The motion planning for the joint trajectories of the NAO humanoid robot done in [3] is based on the Alexander STS (Sit-to-Stand) technique, which focuses on decreasing needed joint torques as the desired joint positions are approached. The proposed STS algorithm has two steps: first, horizontal distances are identified, and secondly, joint angles for putting the robot in a STS position are determined. This is an algorithm that can be applied to all humanoid robots, but the paper focuses on the application for the NAO humanoid robot. Planning an STS motion without falling requires accurate information of the robot's CoM position. Therefore, the calculation of its CoM is performed when the robot is in a sitting position (see Figure 4).

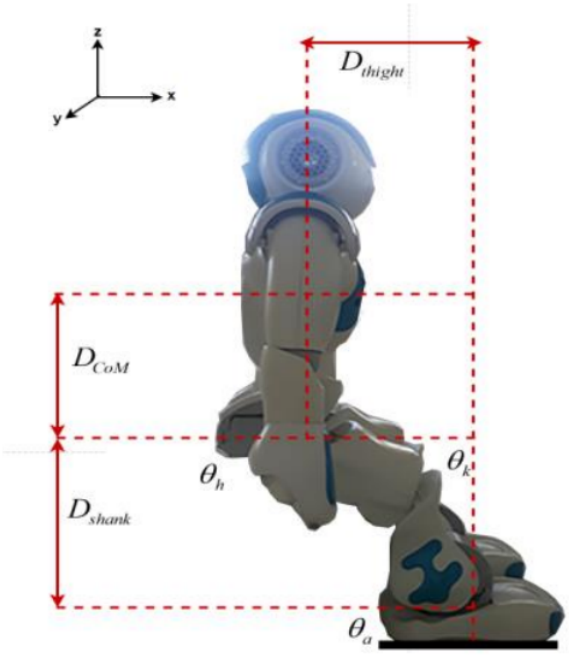

Figure 4: Configuration of the NAO robot at sitting position.

The CoM position of the robot is determined and then desired joint angles for the hip, knee and ankle joints are specified. Furthermore, the obtained joint angles and corresponding body movements for the STS tasks are evaluated. An illustration of the STS cycle can be seen in Figure 5.

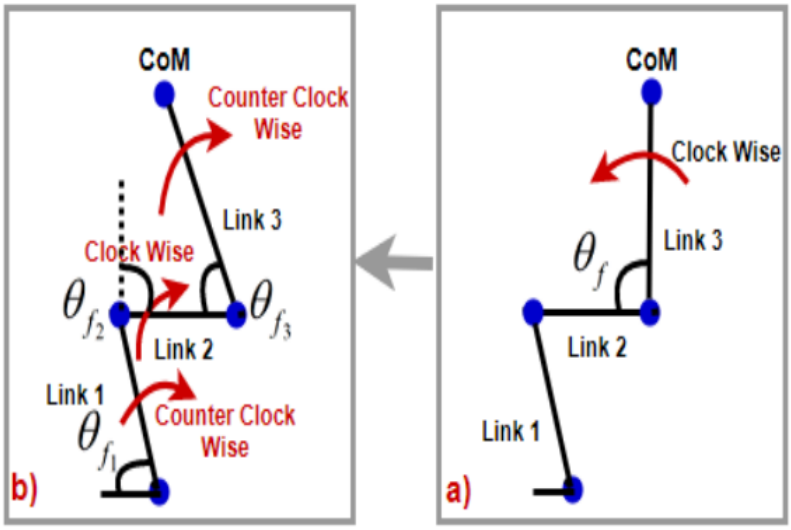

Figure 5: Illustration of an STS cycle. Left: Standing position phase. Right: CoM transferring phase.

3.3.3 Simulation-Based Design of Dynamic Controllers for Humanoid Balancing [4]

Model-based trajectory optimization often fails to find a reference trajectory for underactuated biped humanoid robots performing highly dynamical, contact-rich tasks in the real world due to inaccurate physical models. Therefore, in [4], they propose a complete system that automatically designs a reference trajectory that succeeds on real-world tasks with a very low number of real world experiments. They have developed a system that can automatically design reference trajectories for robots to execute transition motions, given in Figure 6.

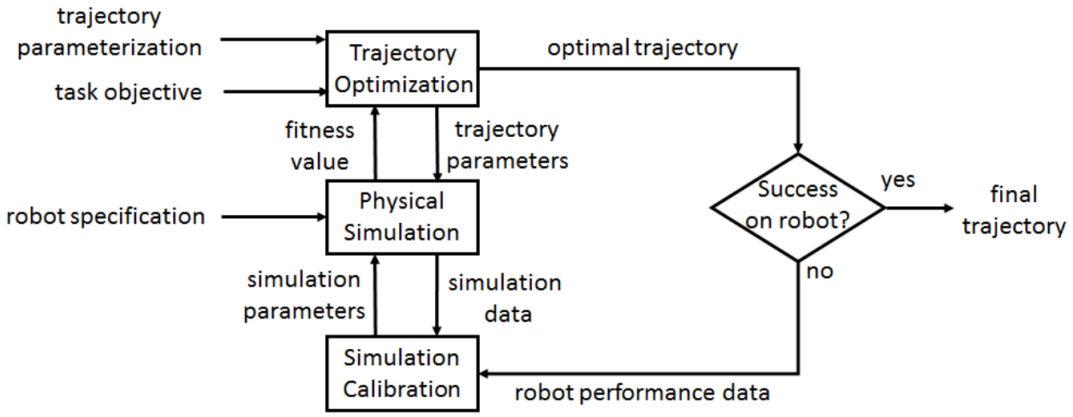

Figure 6: Overview of the algorithm used to automatically design reference trajectories for robots to execute transition motions.

The Physical Simulation block contains the dynamics of the robot model and an actuator model. The robot is modelled as an articulated rigid body system in the simulator, which satisfies the following dynamics equations, as well as non-penetration and linear complementarity conditions for contact points.

$$\begin{aligned} M(q)\ddot{q} + C(q,\dot{q}) &= \tau + J(q)^T f \\ d(q) &\geq 0 \\ d(q)^T f &= 0 \\ f &\in K, \end{aligned}$$

where $M(q)$ is the mass matrix, $C(q, \dot{q})$ is the Coriolis and Centrifugal force, τ are joint torques exerted by the actuators, $J(q)$ is the Jacobian matrix, f is the contact force, $d(q)$ is the distance of the contact to the ground and K is the friction cone. DART is used to solve the above equations to simulate the dynamics of the robot. Furthermore, the derived actuator model based on ideal DC motor assumption and specification of the servo is given by

$$\tau = -k_p(q - \bar{q}) - k_d\dot{q} - k_c\text{sgn}(\dot{q}),$$

where k_p, k_d and k_c are the actuator gains and $\bar{q}$ is the input reference angle.

The Trajectory Optimization block contains trajectory parameterization, a fitness function and optimization with CMA. The reference trajectory $\bar{q}(t)$ is parameterized with a sparse set of keyframes $\{\bar{q}_i\}_{i=0\ldots n}$ at time $\{t_i\}_{i=0\ldots n}$. The first $\bar{q}_0$ and last keyframes $\bar{q}_n$ are given, but the final time $T = t_n$ is optimized. Furthermore, the following fitness function is used to reward the trajectories that keep the robot balanced throughout the entire motion:

$$\{\bar{q}_i\}_{i=1\ldots n-1}, \{t_i\}_{i=1\ldots n} = \arg\max \int_0^{T+1} \frac{1}{|\alpha(t)| + \epsilon} dt,$$

where α is the angle between the up direction of the robot's torso in the local frame and in the global frame. ϵ is a small positive number to prevent the denominator from being zero and $T = t_n$ is the time when the robot reaches the final pose. Finally, a sample-based stochastic optimization algorithm, CMA, is applied to overcome discrete contact events, since this causes problems for continuous optimization algorithms which rely on gradient information.

Even though the optimal reference trajectory $\bar{q}(t)$ can work effectively in simulation, it could still fail in the real world. Therefore, in the Simulation Calibration block, an optimization is formulated which searches for the simulation parameters θ to minimize the discrepancy between the simulated results and the robot performance in the real environment. The optimization is given by

$$\theta = \arg\min \frac{1}{n} \sum_{i=1}^{n} \int_0^{T+1} \|\tilde{q}_i(t) - q_i(t;\theta)\|^2 W dt,$$

where $q(t;\theta)$ is the sequence of simulated robot states with simulation parameter θ. $\tilde{q}_i(t)$ is the real robot states by executing the same reference trajectory, and W is a weight matrix which encapsulates the relative importance of each joint.

4 Results

This section covers some results from the following models: the 3DOF model, with an attempt at replicating some of the results presented in [1] (see section 4.1); the proposed extended model with an added degree of freedom for actuated arms (see section 4.2); and a few other papers on the topic of sit-down/stand-up for humanoid robots (see section 4.3).

4.1 3DOF Model

A numerical search for a minimum of the optimization index (12) yields many motions of the system (8) that satisfy the constraints i-vii. In addition, these motions result in a phase portrait for the motion generator (11) that share the features of the MG for a human, as seen in [16]. These results are noteworthy since

- the number of constraints in the search is greater than the number of parameters k_{ij}, and
- none of the constraints i-vii and the constraints given in **Statements 1-2** for unknown coefficients k_{ij} impose any bounds on the absolute values of the coefficients; $|k_{ij}|$.

One of the found solutions of the robot's sit-down motion was found by choosing the coefficients k_{ij} of (9)-(10) as

$$\begin{aligned} k_{01} &= 0.1491 & k_{02} &= 5.3706 \\ k_{11} &= -4.1356 & k_{12} &= 2.7654 \\ k_{21} &= -4.6977 & k_{22} &= 2.4232 \\ k_{31} &= -0.400 & k_{32} &= 0.2500 \end{aligned}$$

which results in (11) having no equilibrium on the interval $(1, 1.5)$ [rad]. The part of the phase portrait we are interested in is shown in Figure 7, denoted as the *region of interest*. The part of the trajectory (blue curve) which crosses the end of the region of interest in its corner, is the one chosen for reconstructing a sit-down motion for the robot. As seen in the figure, along this trajectory the angular velocity of the ankle $\dot{q}_p$ is first sharply decreasing, until it reaches a minimum value of about -1.2 [rad/s]. Then, it starts to grow until it reaches a steady state value of about -0.8 [rad/s]. We can from this observation conclude that the angular acceleration $\ddot{q}_p$ is small at the end of the motion, which means that property II observed for human behaviours holds for the robot's motion as well.

From Figure 7 we can observe that other trajectories initialised from points nearby the beginning of the curve we discussed also experience similar behaviours, and come to a similar steady state value of the angular velocity $\dot{q}_p$. As for human motion, the trajectory is a part of one of the cycles of the system (11) around its equilibrium, which fulfills feature IV. The nominal external torques $\tau_p^\star$, $\tau_{a1}^\star$ and $\tau_{a2}^\star$ for ankle, knee and hip joints, respectively, that shape the found motion are given in Figures 8-10. From these figures we see that τ_p for the ankle joint stays close to zero, τ_{a1} for the knee joint barely exceeds 75 [Nm] and τ_{a2} for the hip joint stays within ± 80 [Nm]. Also, the motion takes about 0.4 seconds. This means constraints iv, vi and vii are upheld, while v is slightly exceeded. A configuration of the robot, showing a sequence of postures for a found sit-down motion, is given in Figure 11. Note that this configuration is not for the found sit-down motion discussed in this section, but for one found in [1]. The figure is included to show how the motion of the robot can look after finding the dynamics for the system (8). A configuration of the robot for the found sit-down motion discussed in this section was unfortunately not found.

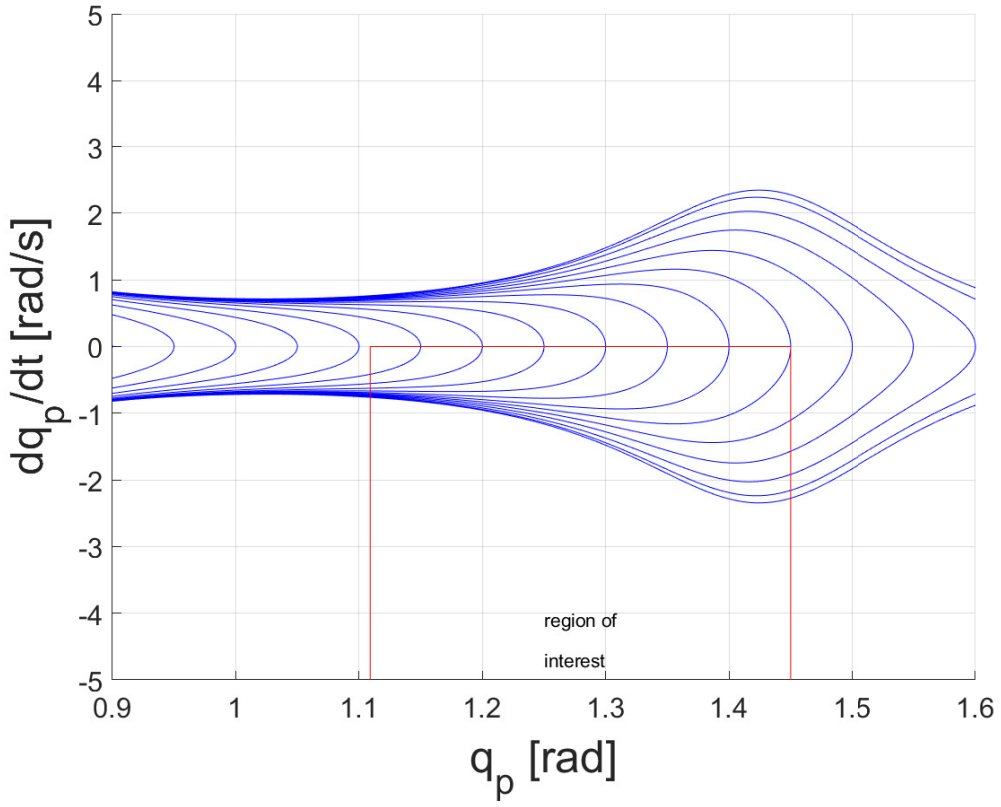

Figure 7: The phase portrait for the system (11) when the coefficients of (9)-(10) are chosen as suggested. The part of the trajectory (blue curve) which crosses the end of the region of interest in its corner, is the one chosen for reconstructing a sit-down motion for the robot. Looking at the entirety of this trajectory (both in and outside of the region of interest), we see that the human motion is a part of one of the cycles of the system (11).

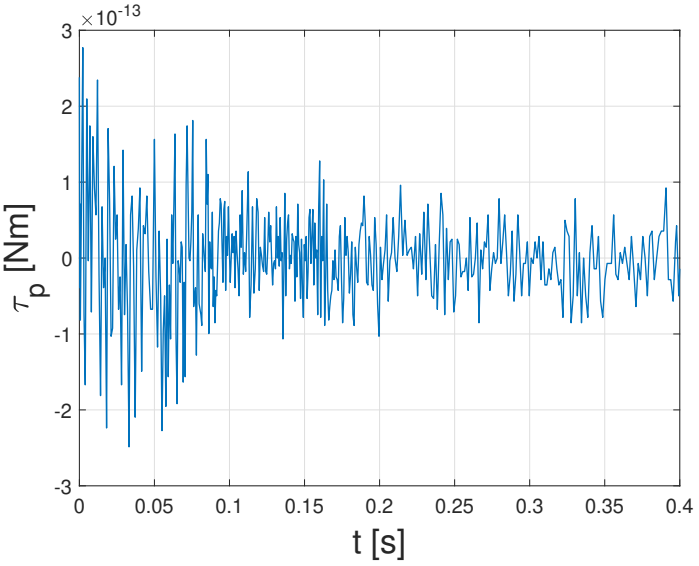

Figure 8: Nominal external torque $\tau_p^\star$ for the ankle joint.

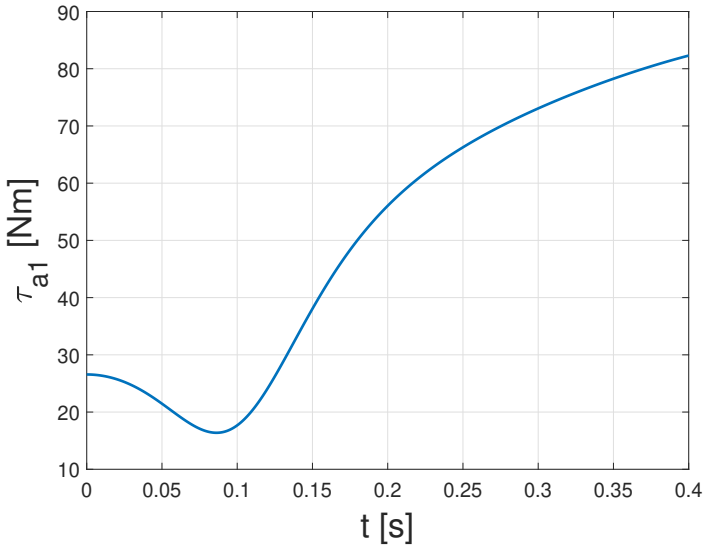

Figure 9: Nominal external torque $\tau_{a1}^{\star}$ for the knee joint.

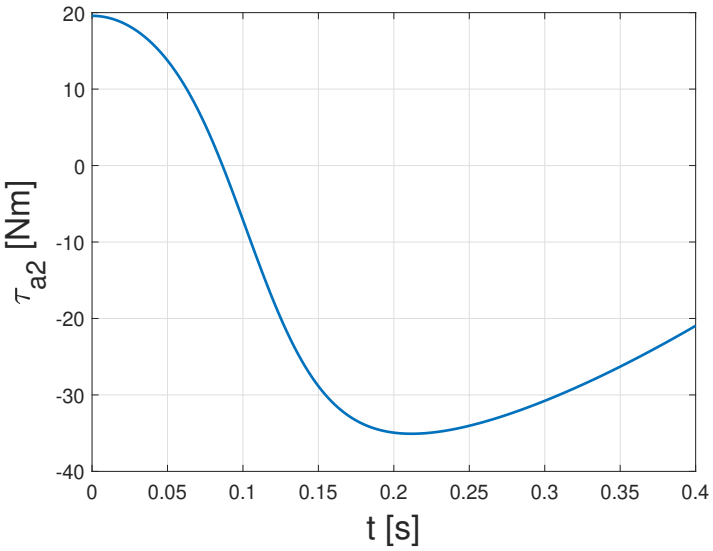

Figure 10: Nominal external torque $\tau_{a2}^{\star}$ for the hip joint.

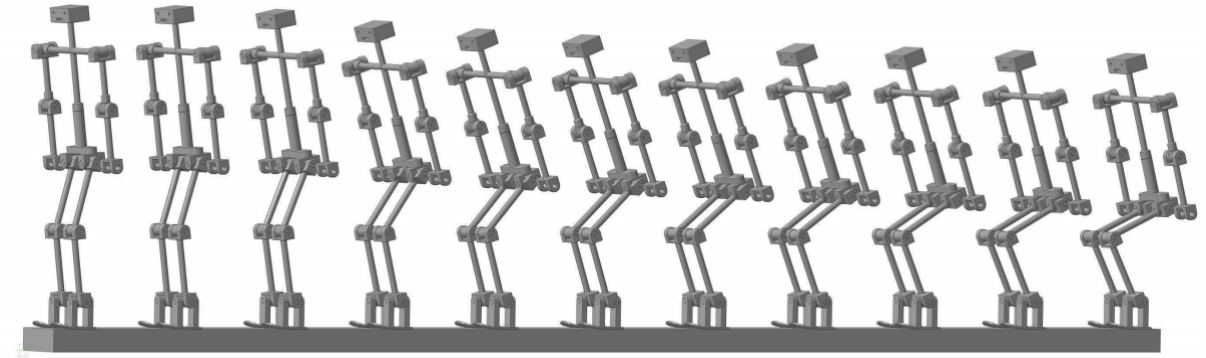

Figure 11: Consecutive configurations of the robot for a found sit-down motion of the system (11). [1]

4.2 Extension of the Model - 4DOF Model with Actuated Arms

An extension of the 3DOF model given in section 3.1 was proposed in section 3.2. Here, a degree of freedom for the angle of actuated arms was added to the 3DOF model, to give the resulting 4DOF model as seen in (16).

Optimization of the robot's sit-down motion by minimizing the values of control torques for the actuated angles, subject to the constraints given in sections 3.1.2 and 3.2.2, yielded many different results. One of the found solutions of the sit-down motion was found by choosing the coefficients k_{ij} of (9), (10) and (17) as

$$\begin{aligned} k_{01} &= -0.3999 & k_{02} &= 0.2497 & k_{03} &= -0.0803 \\ k_{11} &= -4.6959 & k_{12} &= 6.2351 & k_{13} &= -1.0081 \\ k_{21} &= 2.5189 & k_{22} &= -4.3478 & k_{23} &= 4.5351 \\ k_{31} &= -0.0892 & k_{32} &= -4.4260 & k_{33} &= -6.6682 \end{aligned}$$

which results in (18) having no equilibrium on the interval (1, 1.5) [rad]. The part of the phase portrait we are interested in is shown in Figure 12, denoted as the *region of interest*. The part of the trajectory (blue curve) which crosses the end of the region of interest in its corner, is the one chosen for reconstructing a sit-down motion of the robot. As seen in the figure, along this trajectory the angular velocity of the ankle $\dot{q}_p$ is first sharply decreasing, until it reaches a minimum value of about -1.1 [rad/s]. Then, it starts to grow until it reaches a steady state value fo about -0.8 [rad/s]. From this observation we can conclude that the angular acceleration $\ddot{q}_p$ is small at the end of the motion, which means that property II observed for human behaviours holds for the robot's motion in this case as well.

From Figure 12 we also observe that other trajectories initialised from points nearby the beginning of the curve previously discussed also experience similar behaviours, and come to a similar steady state value of the angular velocity $\dot{q}_p$. For human motion, the trajectory is a part of one of the cycles of the system (18) around its equilibrium, which fulfills feature IV. The nominal external torques τ_p, τ_{a1}, τ_{a2} and τ_{a3} for ankle, knee, hip and arm joints, respectively, that shape the found motion are given in Figures 13-16. From these figures we see that τ_p for the ankle joint stays close to zero, τ_{a1} for the knee joint barely exceeds 75 [Nm], while τ_{a2} for the hip joint stays within ± 80 [Nm] and τ_{a3} for the arm joint stays within ± 50 [Nm]. Moreover, the motion still takes about 0.4 seconds. This means constraints iv, vi and vii are upheld, while v is slightly exceeded. Additionally, constraint 2 for arms is also upheld.

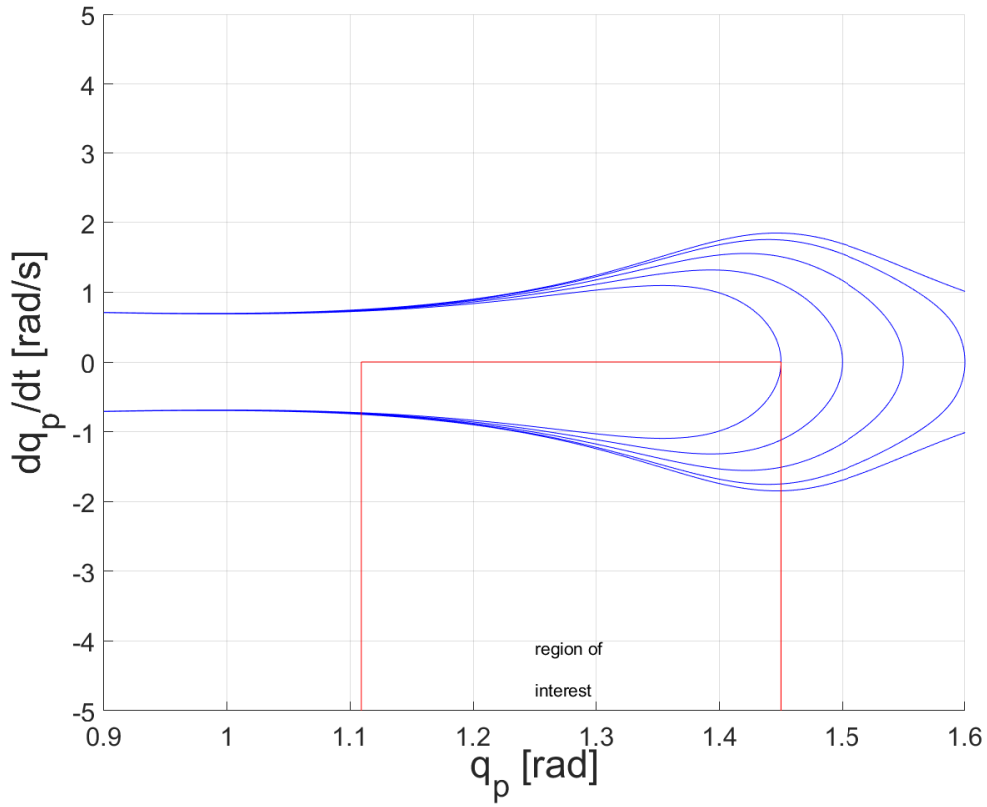

Figure 12: The phase portrait for the system (18) when the coefficients of (9), (10) and (17) are chosen as suggested. The part of the trajectory (blue curve) which crosses the end of the region of interest in its corner, is the one chosen for reconstructing a sit-down motion for the robot. Looking at the entirety of this trajectory (both in and outside of the region of interest), we see that the human motion is a part of one of the cycles of the system (18).

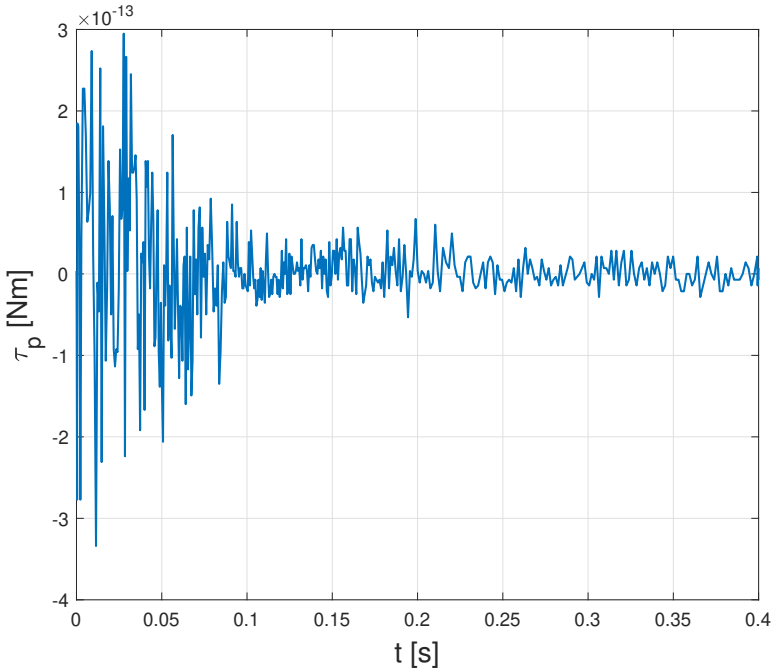

Figure 13: Nominal external torque $\tau_p^\star$ for the ankle joint for the 4DOF system.

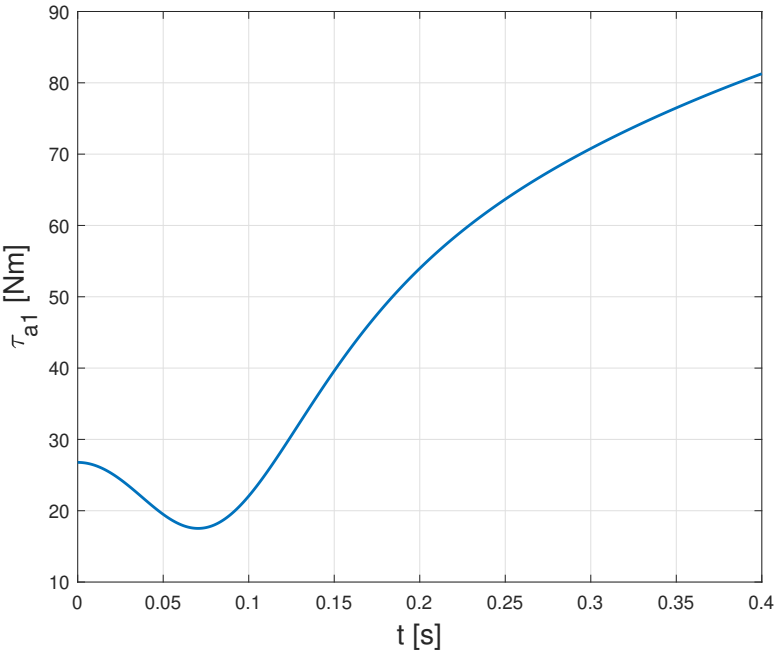

Figure 14: Nominal external torque $\tau_{a1}^\star$ for the knee joint for the 4DOF system.

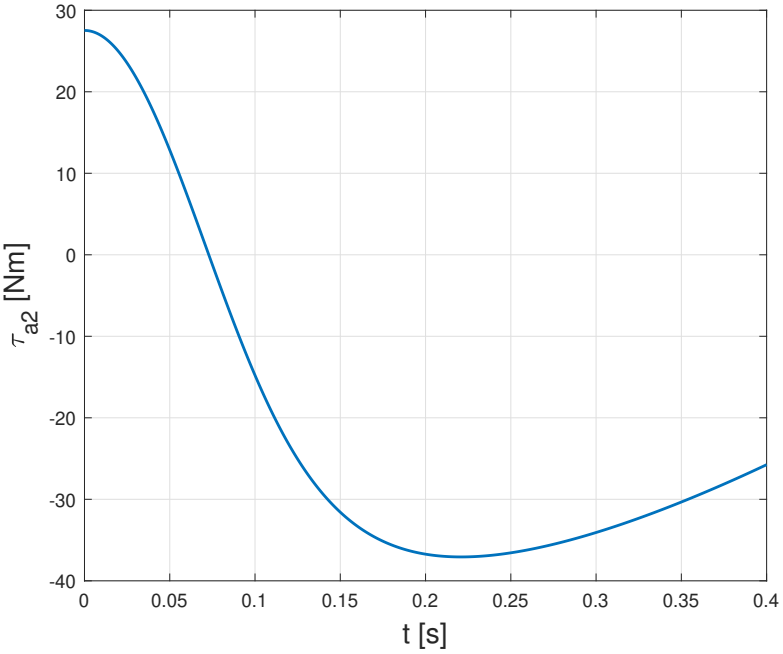

Figure 15: Nominal external torque $\tau^{\star}_{a2}$ for the hip joint for the 4DOF system.

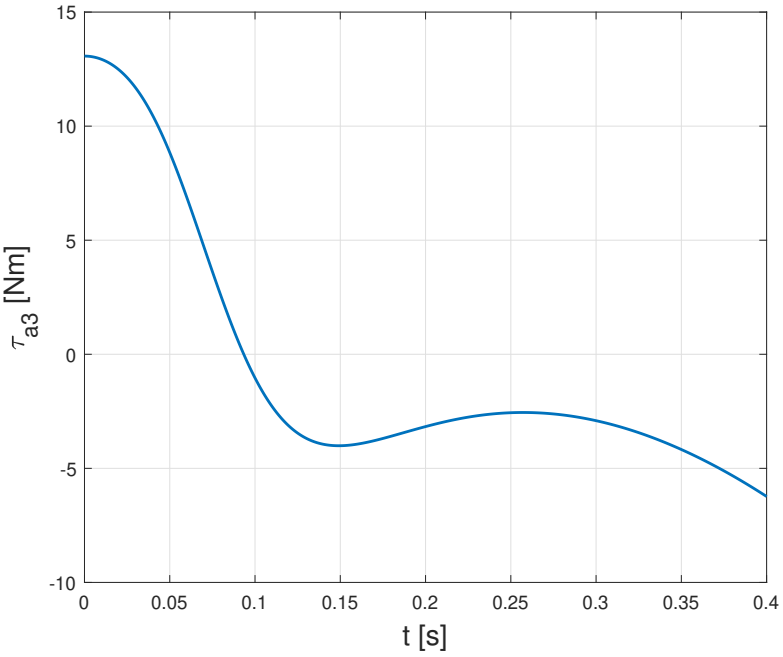

Figure 16: Nominal external torque $\tau^{\star}_{a3}$ for the arm joint for the 4DOF system.

4.3 Other Papers on the Topic

The most important results from papers [2], [3] and [4] are presented in this section. The motion planning procedures for a humanoid robot's stand-up from these papers are given in section 3.3. For further discussion of these results, and comparison with the work done in this paper, see section 5.4.

4.3.1 Sit-to-Stand Task on a Humanoid Robot from Human Demonstration [2]

In [2], human motions were recorded using the VICON optical motion capture system, and simultaneously measuring ground contact force with AMTI force plates. During motion capture, the demonstrators were asked to not move their feet during the stand-up motion, and not touch their hands to the chair or their body. Several healthy people executing natural standing motions were recorded, and also a professional actor performing stylized standing motions, including an imitation of an elderly person. After motion capture, the corresponding robot motion was generated using the estimated CoM parameters for the robot, and the proposed inverse kinematics computations. The planned trajectory was finally executed, at full speed, on the Carnegie Mellon/Sarcos humanoid robot, via joint PD control. An example motion sequence is given in Figure 18, where the professional actor is performing an elderly style stand-up motion, shown at the top of the figure. At the bottom of the figure, we see the corresponding robot sequence generated by the proposed method. The humanoid robot successfully realizes the human motion, as seen in the figure, while maintaining balance during the entirety of the motion.

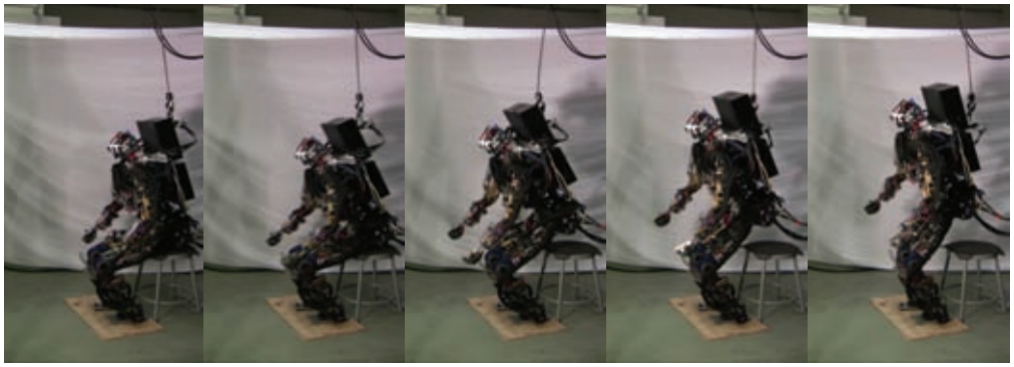

Figure 17: Sequence of a natural standing motion implemented on the humanoid robot.

Figure 19 shows CoM and CoP (Center of Pressure) positions in the longitudinal direction, plotted against time, for an example of a natural standing motion shown in Figure 17. The vertical axis represents the CoM and CoP position [m] with respect to the left foot position, and a positive value represents the forward direction.

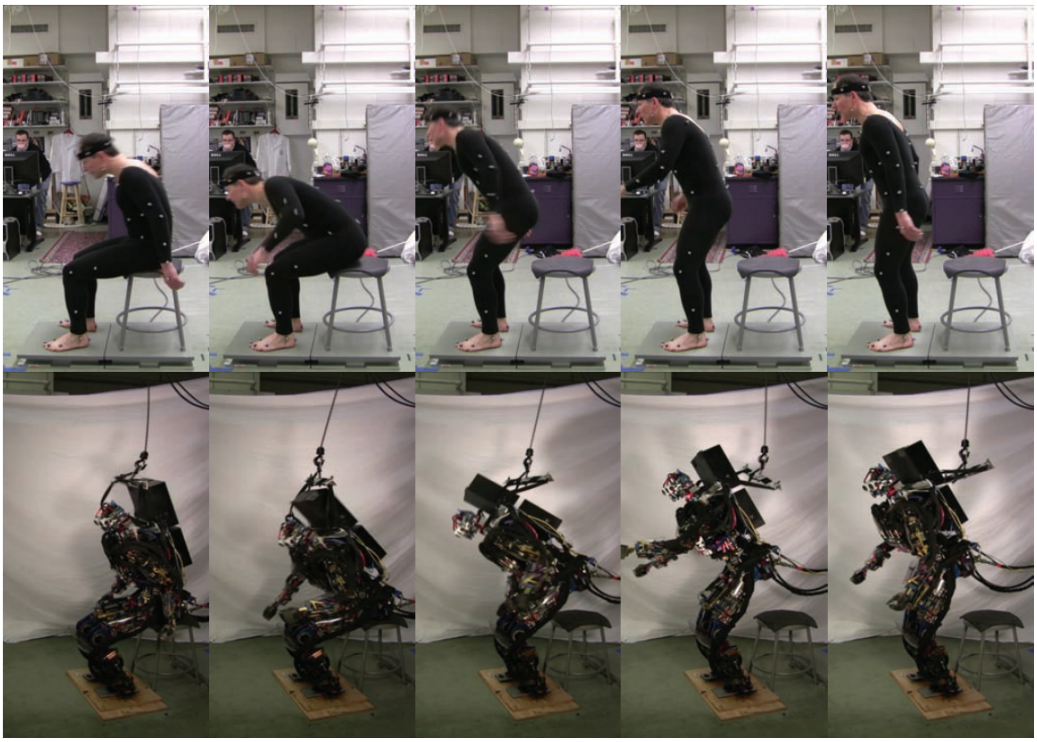

Figure 18: Top: Sequence of a human actor performing an elderly style stand up motion. Bottom: The corresponding humanoid robot's stand up motion when emulating the actor's performance.

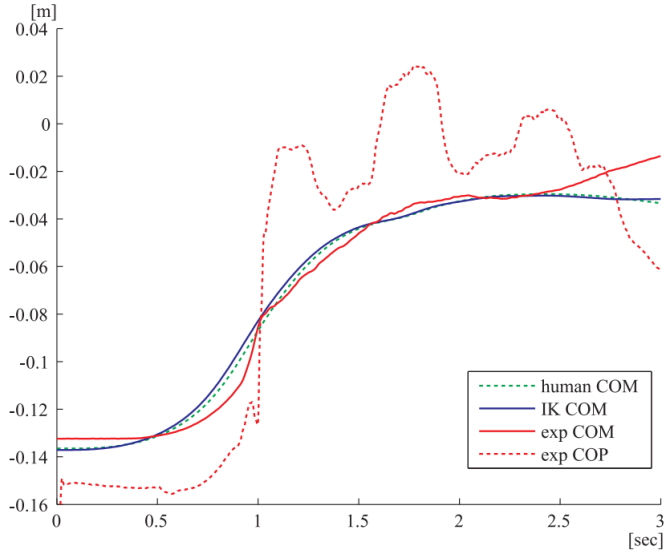

Figure 19: CoM and CoP positions in the longitudinal direction along time, for a natural stand-up motion. Lift-off from the chair occurs at ≈ 1 [sec]. Green dashed line: Human CoM position estimated from the experimental human motion data. Blue solid line: Planned CoM position for the generated humanoid robot motion. Red solid line: Estimated CoM position of the robot during the experiment. Red dashed line: Recorded CoP position of the robot during the experiment.

4.3.2 Sit-to-Stand Motion Analysis for NAO Humanoid Robot [3]

In [3], motion planning for 3 joints is addressed; the coordinated movements of hip, knee and ankle. These joints were analysed, and leg and arm joints played a role in balancing the robot during sitting down and standing up motions, as described in Figure 20.

Block	Used Joints
Left Arm	LSHoulderRoll, LShoulderPitch, LElbowYaw, LWristYaw, LElbowRoll
Right Arm	RSHoulderRoll, RShoulderPitch, RElbowYaw, RWristYaw, RElbowRoll
Left Leg	LHipYawPitch, LHipPitch, LKneePitch, LAnklePitch, LAnkleRoll, LHipRoll
Right Leg	RHipYawPitch, RHipPitch, RKneePitch, RAnklePitch, RAnkleRoll, RHipRoll

Figure 20: The joints to be controlled with the Sit-To-Stand (STS) motion algorithm.

After finding CoM position and transferring phases have been completed, the Sit-to-Stand (STS) motion algorithm is conveyed to the NAO robot's interface through a program called Choreographe. As seen in Figure 21, the desired trajectories obtained from the STS motion algorithm can be applied to a NAO humanoid robot in a real-life experiment.

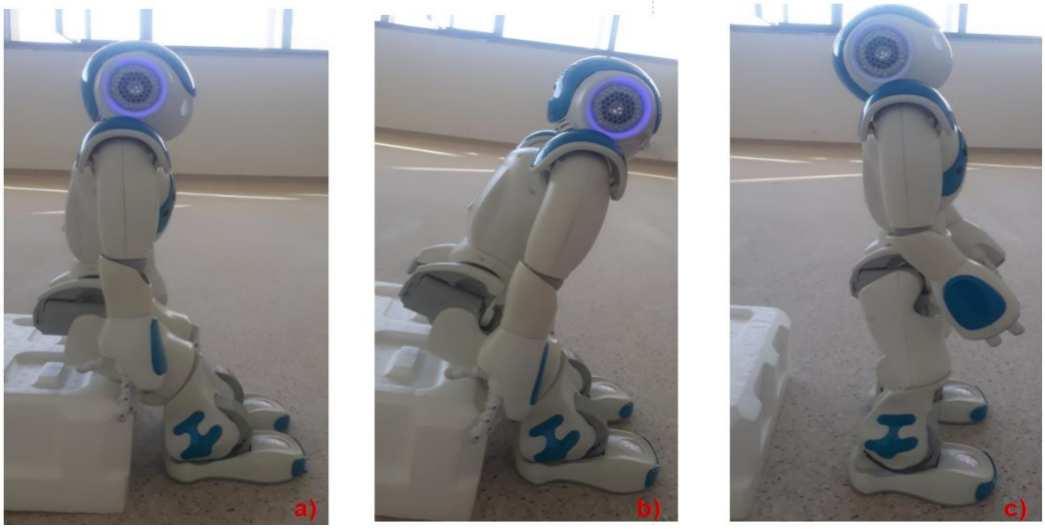

Figure 21: The resulting behaviour of the NAO humanoid robot when using the STS motion algorithm. a) The NAO robot is at its initial sitting position. b) The NAO robot prepares itself to stand up. c) The NAO robot successfully transitions into a standing position.

4.3.3 Simulation-Based Design of Dynamic Controllers for Humanoid Balancing [4]

The robot platform used for performing the given tasks in [4] was the BIOLOID GP. The hardware includes 22 degrees of freedom (DOFs), whereas 16 of them are controllable by Dynamixel AX-12/AX-18 servos. The remaining six DOFs, which indicate the torso position and orientation, are unactuated. To control the robot, a master program on the computer writes the reference pose $\bar{q}$ to the serial port connected to the robot. A slave program which runs on the robot's onboard microprocessor listens to the port, and sends the reference joint angle to each actuator. Simultaneously, the robot performance data $\tilde{x}$ is measured and sent back to the computer. The task from [4] which is covered in this section, is the robot rising from a sitting position, since this is the most relevant to the work done in this paper. In Figure 22, we see the results of the given sit-to-stand task, both from simulation and from the real robot. The initial and final poses q_0 and q_2 are shown in the leftmost and rightmost images in the figure. The trajectory optimization needs to search for an additional inbetween keyframe q_1, as well as the time t_1 and t_2 of these keyframes. The method successfully computes a reference trajectory that enables the robot to stand up in the simulation; the robot first produces a forward momentum by quickly leaning its upper body

to the front. Furthermore, it extends the hips and the knees at the moment when the center of mass (CoM) is moving towards the supporting feet. When the computed trajectory is applied to the hardware, the robot is able to rise successfully without needing simulation calibration. Hence, the "Reality Gap" as it is named in [4], does not always pose a problem.

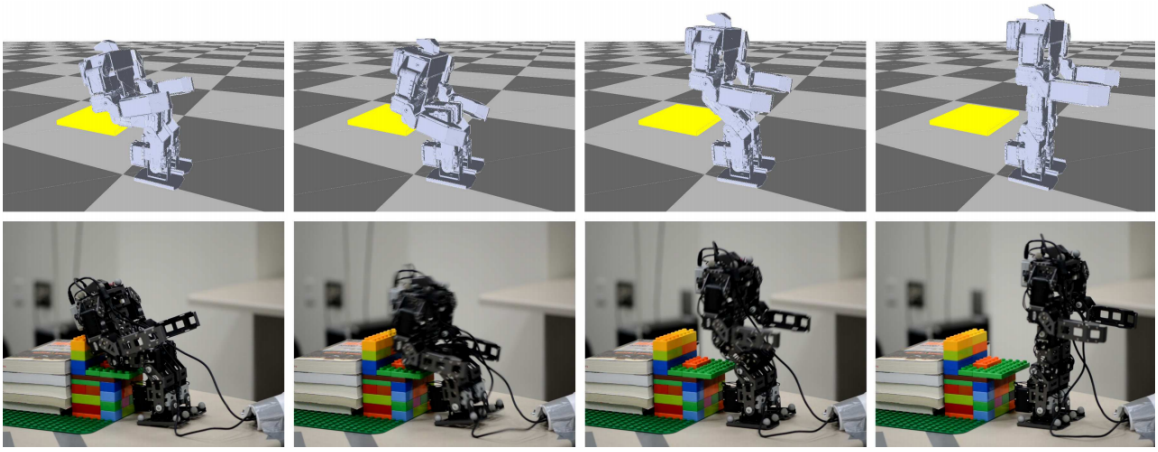

Figure 22: The results of the sit-to-stand task. Top: The task being performed in the simulation. Bottom: The real robot performing the task.

5 Discussion

The results presented in section 4 are further discussed in this section. This includes discussion of results for the 3DOF model (see section 5.1), the extended 4DOF model with an added degree of freedom for actuated arms (see section 5.2) and from other relevant papers (see section 5.4). In addition, some of the results presented in [1] that are not yet mentioned in this paper are also discussed, as well as possible further extensions of the model (see section 5.3).

5.1 3DOF Model

The found sit-down motion presented in section 4.1 was an attempt at replicating some of the results presented in [1], since the 3DOF model from [1] was used as a basis for all work presented in this paper. Some of the original results presented in this paper were satisfactory, and seemed to meet the expectations for a human-like motion given in I-IV (from section 3.1.2). In addition, the results were also somewhat similar to the results reported in [1]. An example of this was the phase portrait given in Figure 7. One could draw some of the same conclusions from this phase portrait as the one reported in [1] for the same 3DOF system, e.g. that along the trajectory chosen for reconstructing a sit-down motion for the robot, the angular velocity $\dot{q}_p$ is first sharply decreasing until it reaches a minimum value, and then it grows until it reaches a steady state, which coincides with feature II observed for human behaviours. The phase portrait from [1] is given in Figure 23, and comparing it to the phase portrait found in Figure 7, we observe a similar behaviour.

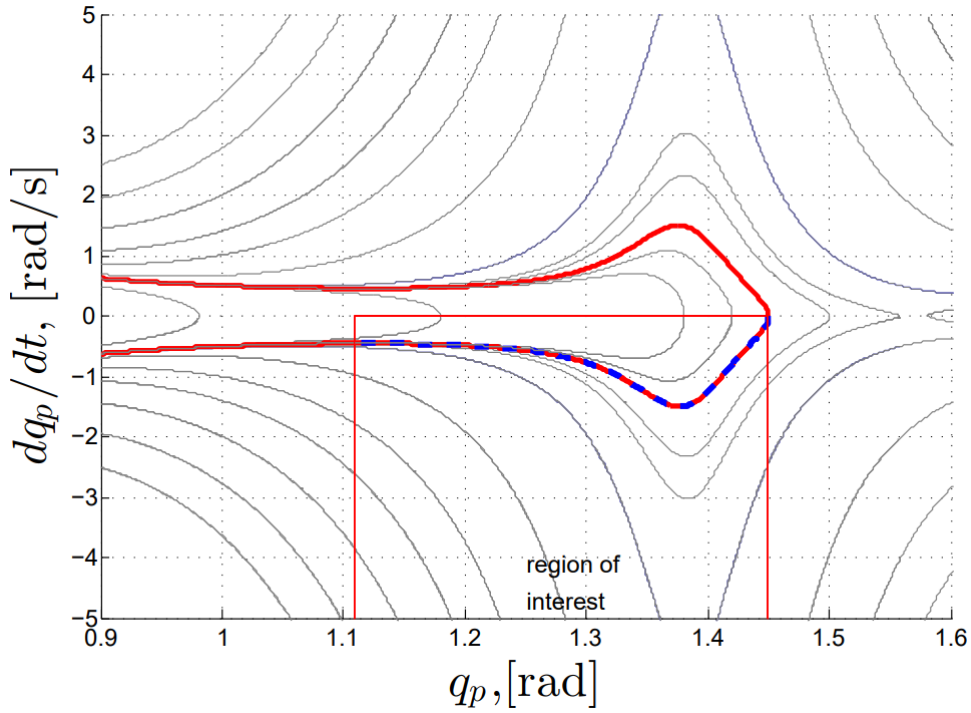

Figure 23: The phase portrait for the system (11) when the coefficients of (9)-(10) are chosen as in [1]. The dashed-blue solution is chosen for reconstructing a sit-down motion for the robot. As for the human motion, it is part of one of the cycles of the system (11), depicted in red. Taken from [1].

While the phase portrait from section 4.1 seemed satisfactory, some other behaviours did not seem up to par with what was presented in [1]. One example of this was the nominal torques, especially the one for the knee joint $\tau_{a1}^{\star}$. From constraint v observed for human behaviours, the torque for the knee joint should not exceed ± 75 [Nm], but from Figure 9 we see that it clearly reaches a value greater than 80 [Nm]. This might be because the coefficients k_{ij} for (9) were not found properly, e.g. as a result of the required constraints not being properly implemented; or

possibly the coefficients k_{ij} for the virtual holonomic constraints of the system, see 3.1.3, could be further tuned. Furthermore, by plotting the nominal angles $q_p^\star$, $q_{a1}^\star$ and $q_{a2}^\star$, we observe that the evolutions of these coordinates do not correspond with the behaviours expected for human motion, from constraints i-iii. This may be because in the given programs (the programs received from Pchelkin, the creator of the model and author of [1]), the initial value for angle q_p was set to $\frac{\pi}{2} - 1.45 \approx 0.12$ [rad]. From this it is hard to fulfill feature i, since the ankle angle q_p will start at around 0.12, and not 1.5 [rad], as seen in Figure 24. So, there was an attempt of changing the initial value for ankle angle to 1.5 [rad], but this made the programs run extremely slowly, and there were no reasonable results. The reason the ankle angle in the given programs was set to ≈ 0.12 [rad] may be because a different frame (than the one where the ankle angle starts at 1.5 [rad]) was in mind. This might also explain e.g. why the ankle angle q_p increases monotonically instead of decreasing (constraint i says it is expected to decrease monotonically).

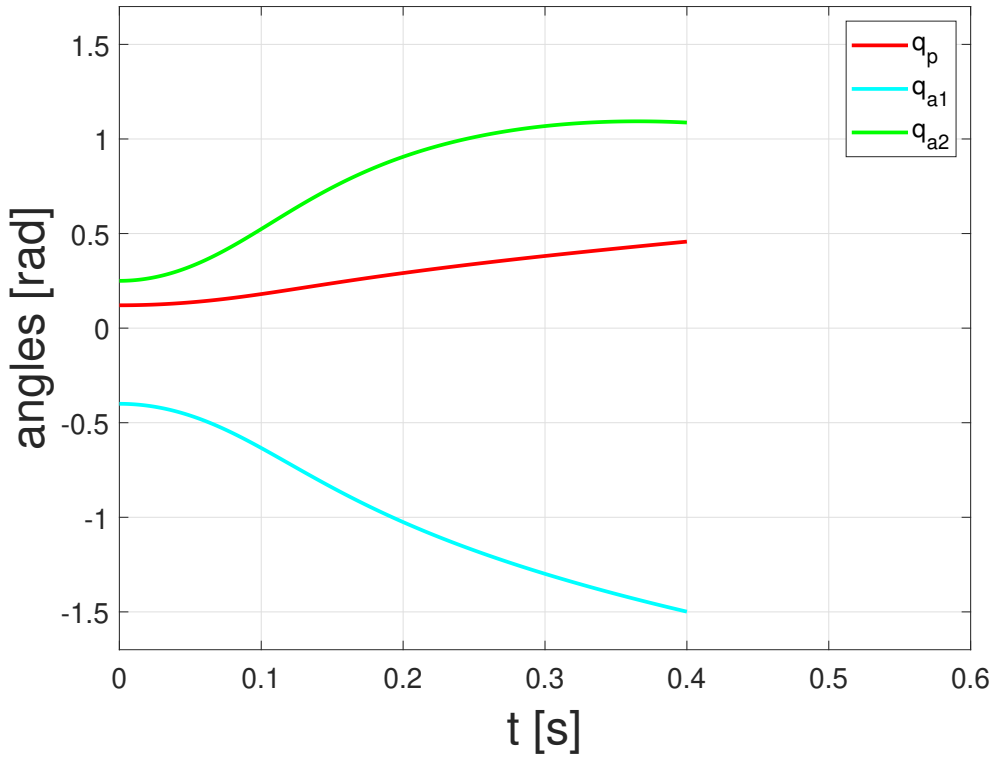

Figure 24: Nominal time evolution of coordinates $q_p^\star$, $q_{a1}^\star$ and $q_{a2}^\star$ for the found sit-down motion of the system (8) given in section 4.1.

5.1.1 Example of Handling Perturbations of the Motion Generator

An interesting thing about the motion planning procedure presented in section 3.1, is how flexible it can be in handling perturbations. In [1], it is observed that the vertical component of the ground reaction force F_y reaches a negative value at some point during the found sit-down motion. In practice, this means the legs should lift off the ground at this point in time, which is inconsistent with the assumptions made while building the model (6). The simplest way of handling such an inconsistency is to rewrite the expression for the ground reaction force in terms of q_p, $\dot{q}_p$ and coefficients k_{ij}, and requiring that the orbit of a candidate motion does not intersect with curves, where the expression is zero. However, the situation is handled by salvaging the already found solution and introducing a dynamical extension of the model. A non-trivial behaviour of the robot arms is included into the search, to be responsible for satisfying the reaction force constraint. The arms are assumed to move identically in the sagittal plane, and the dynamics take the same form as the extended model given in (16), where q_{a3} is the angle for actuated arms. The new MG takes

the same form as (18), and new constraints are added: the ground reaction force F_y has to keep its sign, and q_{a3} needs to be within a reasonable range. By minimizing $\{|\tau_{a1}|^2 + |\tau_{a2}|^2 + |\tau_{a3}|^2\}$, and keeping $F_y > 0$ and $q_{a3} \in [-\frac{\pi}{2}, \frac{\pi}{2}]$, while keeping all the constraints from the previous search (procedure for 3DOF model) active, a solution for the extended model can be found. The phase portrait of the perturbed MG ended up sharing the same features found in the analysis of the human performance, just like for the MG for the 3DOF system (11). This means that despite the increase in order of the model, the phase portrait of the MG remained very close to the one derived for the 3DOF model (8). Also, the coefficients of the two MGs remained very close to each other, which shows a structural robustness of the suggested motion planning procedure. Additionally, the existence of a dynamic human-like motion along the virtual holonomic constraints confirms the assumption of passivity of the ankle joint. If a non-zero torque in the ankle joint was necessary for executing the motion, the dynamical motion with zero ankle torque would not have existed along the VHCs.

5.2 Extension of the Model - 4DOF Model with Actuated Arms

The proposed extension of the original 3DOF model presented in section 3.1, is the 4DOF model with an added degree of freedom for actuated arms, presented in section 3.2. Motion planning of this extended model required adding a degree of freedom to the dynamics of the model, and finding a new motion generator from these new dynamics. In addition, new coefficients for (9), (10), as well as coefficients for arm evolution (17), had to be found. This might seem similar to what was discussed in section 5.1.1, where a degree of freedom for actauted arms was added to the already established 3DOF model, to try and handle the given perturbations. The difference between these two approaches is that in the extended model presented in section 3.2, all the coefficients of (9), (10) and (17) were searched for simultaneously, with all constraints active at once, instead of separately searching for coefficients of (17) and adding these results to the already found results of the 3DOF model.

The purpose of extending the 3DOF model given in [1] (see section 3.1) by adding a degree of freedom, is to further increase the complexity of the model, and simultaneously move one step closer to a model that works for all specifications and perturbations. By increasing the complexity, the model also moves one step closer to being realized into an actual humanoid robot, or even a wearable robotic device such as an exoskeleton. For a humanoid robot or an exoskeleton to actually be of any use in a practical setting, they would most likely need to have more than three, or even four, degrees of freedom.

From the results of our extended 4DOF model given in section 4.2, we seem to have met the expectations for a human-like motion given in I-IV (from section 3.1.2). The results were quite similar to the results for the 3DOF model found in section 4.1, which again were quite similar to the results reported in [1]. By observing the phase portrait for our 4DOF model from Figure 12, we see that along the trajectory chosen for reconstructing a sit-down motion for the robot, the angular velocity $\dot{q}_p$ is first sharply decreasing until it reaches a minimum value, and then it grows until it reaches a steady state, which coincides with feature II observed for human behaviours. This is a similar behaviour to what we see in the phase portrait for our 3DOF model (see Figure 7), as well as the phase portrait taken from [1] (see Figure 23).

By comparing the plots for nominal torques of the 4DOF model with the 3DOF model, we see that the ankle torque τ_p still stays close to zero and the knee torque τ_{a1} is almost identical. Meanwhile, the hip torque τ_{a2} starts at about 28 [Nm] for the 4DOF system, and drops down to a minimum of approximately -37 [Nm]. For the 3DOF case the hip torque had extreme values at 20 [Nm] and -35 [Nm], which means we can notice a difference in evolution of our initial three degrees of freedom by adding a degree of freedom for actuated arms. The difference in hip torque is to compensate for the additional degree of freedom added to the model.

Since the nominal torque for the knee joint $\tau_{a1}^{\star}$ for our 4DOF model (see Figure 14) was pretty much identical to the torque for the knee joint of the 3DOF model (see Figure 9), we have that constraint v observed for human behaviours, which says the torque for the knee joint should not exceed ± 75 [Nm], is not upheld. However, the constraint is only slightly exceeded, and need not

be of large significance. For a robot this only means that it's knee joint would have to be able to apply a torque larger than ± 75 [Nm], or alternatively address this with e.g. parallel elastic actuators (see section 5.3.1). However, for a wearable robotic device, such as an exoskeleton, it is important that it does not force the human to apply a torque to some joint larger than what they are physically capable of.

By plotting the nominal angles $q_p^\star$, $q_{a1}^\star$, $q_{a2}^\star$ and $q_{a3}^\star$ for our 4DOF model (see Figure 25), we observe that the evolution of these coordinates do not correspond with the behaviours expected for human motion given in constraints i-iii. However, as previously discussed in section 5.1, this is likely because in the given programs, there are different initial values for the angles, and there is a different frame in mind.

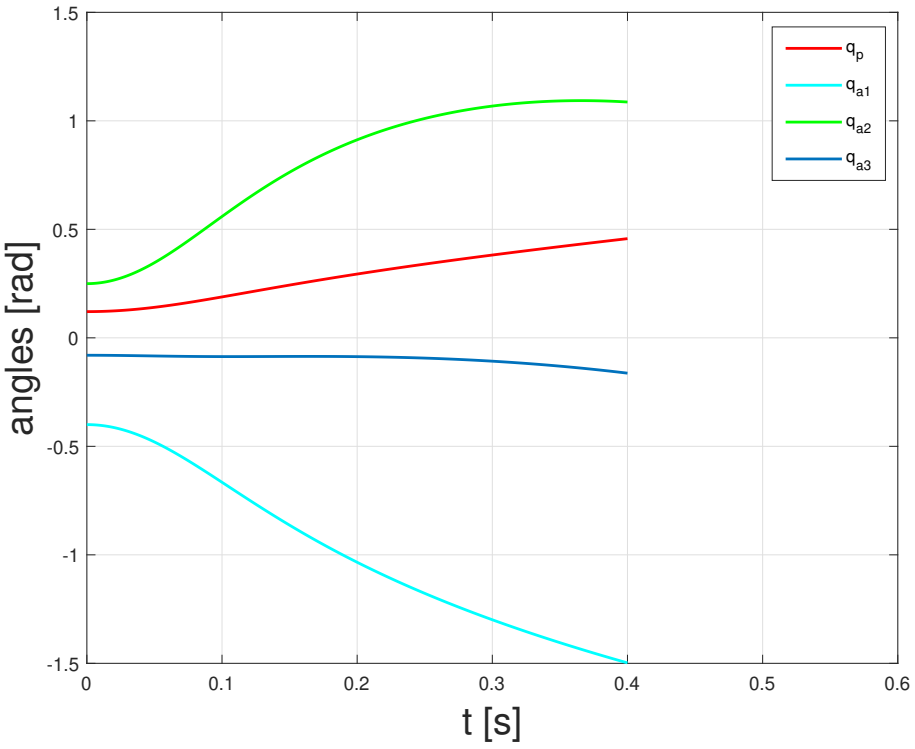

Figure 25: Nominal time evolution of coordinates $q_p^\star$, $q_{a1}^\star$, $q_{a2}^\star$ and $q_{a3}^\star$ for the found sit-down motion of the system (16) given in section 4.2.

Note that the optimization procedure can be done in a number of ways. For example, we can minimize the errors between the angles at the end of the motion and a desired angle. This particular choice was attempted, with the objective function taking the form:

$$F_{new} = |q_{2end} - q_{2T}| + |q_{3end} - q_{3T}| + |q_{4end} - q_{4T}|, \tag{26}$$

where the values q_{iT} could be any choice for desired angles. Also, a number of different constraints were tried out, including additional constraints for angles, angle velocities etc. The results remained more or less the same when adding other reasonable constraints - you could get quite ugly results by adding extremely strict constraints for the angle evolutions of the robot, but there was no need for this in our case. This find is completely reasonable, as the most important part is to find sufficient choices of coefficients k_{ij} for (9), (10) and (17) which give satisfactory sit-down trajectories to be generated by the model.

5.3 Further Work, Extensions and Applications

This section covers suggestions for further work, namely control of the robot's sit-down behaviour (see section 5.3.1), further extensions and also applications of the work done in this paper (see section 5.3.2).

5.3.1 Further Work - Control

When planning a control scheme for a robot sitting down, a feedforward approach seems a lot more fitting than the much used feedback approach. This is because feedback control is typically used to regulate a variable (or variables) in a control systems design with time varying disturbances [17]. Since we have a finite-time motion, in which the robot should successfully go from standing up to sitting down during the short time-span of the procedure, there is little to no benefit to regulating any variables by feedback. Therefore, we suggest a feedforward control scheme for controlling the robot's sit-down behaviour, shown in Figure 26. Here, the nominal torques are used to find nominal angles, in the Preplanned Motion block, which are then inputted into the Controller block. The Controller generates the controlled torques, which are then inputted into the Mechanical Systems block, which contains the dynamics of the 4DOF model. The final output is the controlled angles.

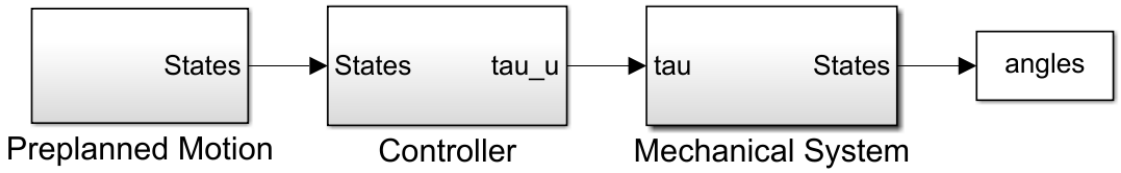

Figure 26: A feedforward control scheme for controlling the robot's sit-down behaviour. The Preplanned Motion block outputs nominal angles for the robot's sit-down behaviour, while the Controller block contains the chosen controller. The Mechanical System block contains the system dynamics, and outputs the controlled states of the system.

When it comes to controller design, i.e. choosing the contents of the Controller block shown in Figure 26, there are a lot of different approaches. In [1], the chosen control procedure for controlling the robot's sit-down behaviour was finite-time contraction to a target orbit via stabilization of transverse dynamics. Moreover, in [18], parallel elastic actuators were used as a control tool for preplanned trajectories of an underactuated mechanical system. Since our model of a robot is also an underactuated one, this is of interest for our case as well. It is mentioned that if some motions are planned that require a nominal control input above the actuator limitations, then we can search for auxiliary spring-like mechanisms complementing the control scheme in order to overcome the constraints [18]. As mentioned in section 5.2, we notice that our constraint which says torque for the knee joint τ_{a1} should not exceed ± 75 [Nm] is not upheld in our test results. This opens up for the possibility of using parallel elastic actuators as a control tool, since we require a nominal torque above the limitations we initially set. However, in [18], the elastic actuators were used in parallel with a feedback controller. We suggest a feedforward control scheme using parallel elastic actuators for controlling the robot's sit-down behaviour, shown in Figure 27. In this block diagram, we see that the nominal angles are inputted into the block Tuned Springs, which contains the dynamics of some chosen springs, as well as the Controller block. Furthermore, the controlled torque of the dynamics is now composed of $\tau = \tau_u + \tau_c$.

5.3.2 Further Extensions and Applications

Some suggested further extensions for the 3DOF model, as seen in section 3.1, could be any model with one or more added degrees of freedom for any body parts receiving change during the given motion. This could be e.g. arms (as seen in section 3.2), neck, legs, spine, torso, etc. Furthermore, the robot does not necessarily need to replicate human behaviour to perform a sit-down; if any unhuman-like configurations make the task easier for the robot, it could be beneficial to let it behave this way. A human usually has a quite linear way of sitting down; by bending the knees, while having a symmetrical behaviour of legs and arms. If a found motion planning procedure for a

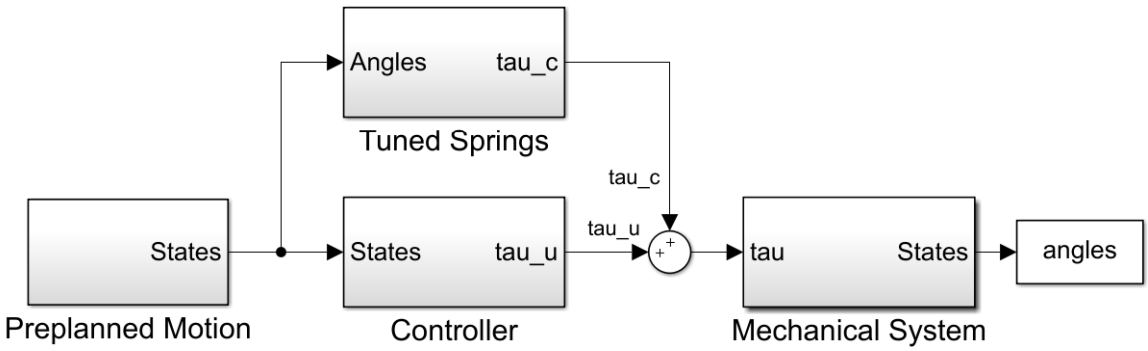

Figure 27: A feedforward control scheme using parallel elastic actuators as a control tool for controlling the robot's sit-down behaviour. The Preplanned Motion block outputs nominal angles for the robot's sit-down behaviour, while the Controller block contains the chosen controller. The Tuned Springs block contains the chosen spring mechanism and the Mechanical System block contains the system dynamics, and outputs the controlled states of the system.

humanoid robot results in the robot having some unhuman-like behaviour during the given motion, e.g. having non-symmetrical behaviour of legs or arms, performing a small hop, or anything else imaginable, why should we not let it act this way? If it were just a robot used by engineers to do research, it shouldn't be a problem to let the humanoid robot act in any way, human-like or unhuman-like. The issue comes with having humanoid robots available to the public, which will be more and more prevalent as time goes on. A humanoid robot which interacts with any and all kinds of people on a day-to-day basis, would preferably act like a human as well, to not cause confusion or fear. If we imagine a robot resembling a human, jumping around and doing all sorts of crazy maneuvers, this could potentially frighten a lot of people. Just imagine *Sophia*, the social humanoid robot developed by Hanson Robotics (see Figure 29) twisting its head around 180 degrees when approached from behind, or jumping to get up a flight of stairs.

Figure 28: The exoskeleton *INNOPHYS* is used by elderly people in Japan to delay retirement. [19]

Additionally, if the procedures generated for a humanoid robot is to be further applied to a wearable robotic device, e.g. an exoskeleton, this device should not twist and turn the human wearing it, outside of what their body is physically capable of. This is of utmost importance to avoid injury, but it should be noted that wearable robotic devices such as exoskeletons do not move on their own, they are designed to move according to the person wearing it. It works more like an extension of the person's body, hence the name *exoskeleton*, which means external skeleton. Exoskeletons are already used by elderly in Japan to delay retirement, as seen in [20]. However, note that exoskeletons come in many different shapes and sizes, and the *INNOPHYS* exoskeleton used for supporting upper muscles, seen in Figure 28, is a lot simpler in concept than the powered exoskeleton shown in Figure 2. The more complex powered exoskeletons are powered by a system of electric motors,

levers, hydraulics etc., and have certain medical, military and industrial applications. They also have civilian applications, and could be very useful for e.g. firefighters and other rescue workers, to help them climb stairs while carrying heavy equipment.

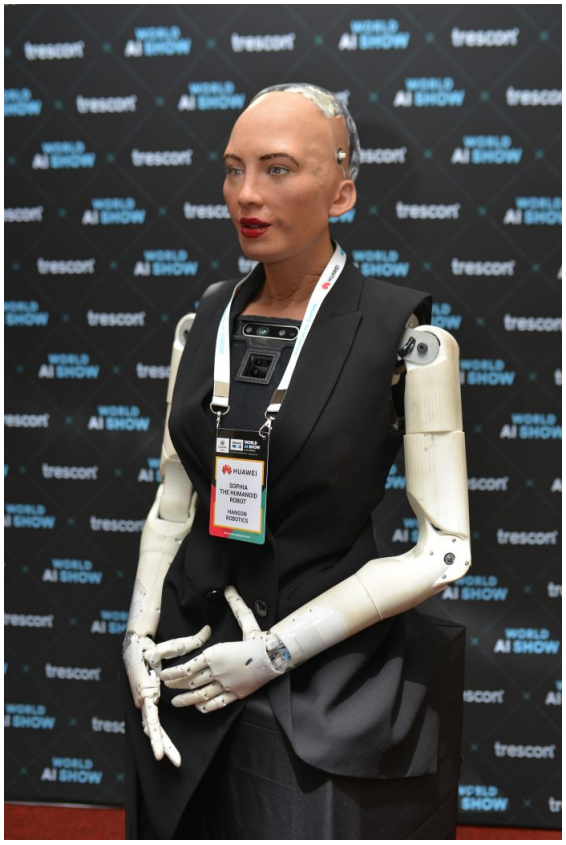

Figure 29: The social humanoid robot *Sophia*, developed by Hanson Robotics. [21]

5.4 Other Papers on the Topic

When planning a motion for a humanoid robot, it seems like a good starting point to record human movements, and make the robot replicate these movements, as done in [2]. Another approach could be to look at previously recorded human behaviours, and use these features as guidelines and constraints on how to plan the robot's movement, as done in [1]. However, using recorded human movements for planning a humanoid robot's motion is not a necessity, as seen in [3] and [4]. Here, human-like behaviour is replicated by properly controlling the robot's motion in the dynamic and unstructured environments. Also, in the papers [2], [3] and [4], the motion planning procedure is for a *stand-up from sitting down position*. This is obviously not the exact same procedure as in this paper, where a sit-down motion for a humanoid robot was regarded. However, a stand-up and a sit-down are not very different by nature. A stand-up from a sitting position could be regarded as a sit-down in reverse, with maybe a few small differences. It was therefore concluded that motion planning and analysis of a stand-up motion was relevant to the topic covered in this paper. One could especially think that the same joints are experiencing change when whether performing a sit-down or a stand-up. This means the same degrees of freedom could be used for planning the motion.

For the CoM parameter estimation done in [2], the model of the robot was reduced to a 5-link model with 4 actuated DOFs for ankle, knee, hip and torso, while the base link remained unactuated. This could be done since these DOFs were the only relevant ones for the sit-to-stand task in question. The dimensionality reduction of the system is similar to what is done in both [1] and [3], where a 28DOF and a 25DOF system, respectively, was reduced to 3DOFs. When the motion

planning procedure was applied to the Carnegie Mellon/Sarcos humanoid robot, the results looked promising. For a natural standing motion, recorded from healthy people, the robot replicated the movement in a similar fashion, as seen in Figure 17. Furthermore, when a professional actor performed an elderly style stand-up motion, the robot had no issues emulating this movement either, as seen in Figure 18. Additionally, from Figure 19 we see that the solid red line follows the green dashed line and the blue solid line, meaning the motion of the humanoid robot realizes the human's CoM trajectory well.

Figure 30: A BIOLOID GP humanoid robot. [22]

In [4], a system which automatically designs reference trajectories for robots to execute transition motions was developed. Furthermore, some given tasks were performed by a biped humanoid robot, both in simulations and in real life. One of these tasks was a rise up from a sit-down position, which is the same task covered in both [2] and [3]. This motion was not planned by emulating human behaviours, as done in [2], nor by using recorded human motions as guidelines and constraints for motion, as done in [1]. Furthermore, the robot used was the BIOLOID GP, which includes 22 DOFs, whereas six of them are unactuated. The simulation calibration approach, which was implemented into the algorithm, was arguably the most impressive feature from [4], but had no use when the robot was performing a sit-to-stand task. The simulation calibration was implemented to reduce the so-called "Reality Gap", which was meant to reduce discrepancy between the simulated results and the robot's performance in a real environment. However, the high degree of freedom system had no problem performing a stand-up from a sit-down position both in simulation and in the real world, with no use of simulation calibration.

When planning the motion for a (NAO) humanoid robot in [3], 3 joints were addressed, namely the coordinated movements of hip, knee and ankle. These are the same 3 DOFs of which the motion was planned for in the base model from [1]. However, note that in [3], the angle for the ankle joint was not assumed completely passive, and the system was not an underactuated one. It is mentioned that produced insufficient ankle torque caused problem during standing up for the NAO humanoid robot, which was addressed by implementing smooth trajectory planning and motion control together. Also, it is mentioned that proper relative movements of the legs and

arms are extremely important for sitting down and standing up for both humans and humanoid robots. When the perturbation is handled by adding a degree of freedom of actuated arms in [1] (see section 5.1.1), some of the same logic is applied. However, unlike [3], planning movements for arms or legs from the beginning was not the approach in [1]. Although, planning the motion for arms from the beginning was the approach for the extended 4DOF model with actuated arms, as proposed in this paper, which did give satisfactory results.

The STS algorithm implemented for the NAO humanoid robot is claimed to be modifiable and possible to implement for all humanoid robots. It should be noted that the NAO humanoid robot has 25 DOFs, while the Mahru III (see Figure 1) has 28 DOFs. This could mean that modifying and implementing the STS algorithm for the Mahru III is not too difficult a task, but it remains to be shown.

Figure 31: An NAO humanoid robot. [23]

6 Conclusion

By looking at several different approaches in motion planning procedures, it is clear that there are many ways to successfully make a robot safely sit down or stand up. One approach for doing this is to first record human behaviours, and then make the humanoid robot emualate said behaviours, as done in [2]. Another approach is to analyse previously recorded human behaviours during a motion, see how the human is expected to perform this motion, and use these features both as constraints and as reference points for the humanoid robot's motion, as done in [1] and in this paper. Moreover, human behaviours do not necessarily need to be directly replicated for planning a humanoid robot's motion, as can be seen in [3] and [4].

The proposed extension of the model presented in this paper, namely the 4DOF model with an added degree of freedom for actuated arms, was successfully implemented and gave satisfactory results. Additionally, the work done in this paper can be further continued; by increasing the model complexity (adding more degrees of freedom), or by e.g. implementing control of the robot's motion. The ideal end goal of extending this model would be to find a model that works for all specifications, parameters and perturbations. By working towards this goal, one can find better and better models, without necessarily reaching the end goal anytime soon.

References

[1] S. Pchelkin, A. Shiriaev, L. Freidovich, U. Mettin, S. Gusev, W. Kwon, and L. Paramonov, "A Dynamic Human Motion: Coordination Analysis," Journal of Biological Cybernetics, 109(1), 2015, pp. 47–62.

[2] M. Mistry, A. Murai, K. Yamane, and J. Hodgins, "Sit-to-Stand Task on a Humanoid Robot from Human Demonstration," 2010 10th IEEE-RAS International Conference on Humanoid Robots, Humanoids 2010, January 2011, pp. 218 – 223.

[3] F. Gongor, O. Tutsoy, D. Barkana, and S. Colak, "Sit-to-Stand Motion Analysis for NAO Humanoid Robot," International Conference on Innovation Trends in Multidisciplinary Academic Research ITMAR. Istanbul, Turkey, October 2017.

[4] J. Tan, Z. Xie, B. Boots, and C. K. Liu, "Simulation-Based Design of Dynamic Controllers for Humanoid Balancing," 2016 IEEE/RSJ International Conference on Intelligent Robots and Systems (IROS), October 2016.

[5] J. Yamaguchi, A. Takanishi, and I. Kato, "Development of a biped walking robot compensating for threeaxis moment by trunk motion," IEEE/RSJ international conference on intelligent robots and systems, July 1993.

[6] J.-Y. Kim, I.-W. Park, and J.-H. Oh, "Walking Control Algorithm of Biped Humanoid Robot on Uneven and Inclined Floor."

[7] CCSI, "Robots: In the beginning." [Online]. Available: http://www.mind.ilstu.edu/curriculum/medical_robotics/robots_in_beginning.php

[8] S. Kerrigan, "Why Are We So Scared of Robots? 15 Experts Weigh In on What the Real Dangers Are," May 2018. [Online]. Available: https://interestingengineering.com/why-are-we-so-scared-of-robots-15-experts-weigh-in-on-what-the-real-dangers-are

[9] U. Mettin, P. La Hera, L. Freidovich, A. Shiriaev, and J. Helbo, "Motion planning for humanoid robots based on virtual constraints extracted from recorded human movements," Intel Serv Robotics, 1, 2008, pp. 289–301.

[10] J. Wakefield, "Exoskeleton that allows humans to work and play for longer," July 2018. [Online]. Available: https://www.bbc.com/news/technology-44628872

[11] K. Aken, "Powered Exoskeletons Make the Jump from Sci-fi, to Plain Sci," October 2016. [Online]. Available: https://www.technologypep.com/powered-exoskeletons-make-the-jump-from-sci-fi-to-plain-sci.html

[12] W. Kwon, H. Kim, J. Park, C. Roh, J. Lee, J. Park, W. Kim, and K. Roh, "Biped humanoid robot Mahru III," IEEE-RAS 7th International Conference on Humanoid Robots. Pittsburg, USA, 2007.

[13] U. Mettin, "Principles for Planning and Analyzing Motions of Underactuated Mechanical Systems and Redundant Manipulators," Department of Applied Physics and Electronics, Umeå University, 2009.

[14] A. Shiriaev, "Lecture notes: Oscillations of nonlinear systems," Lund University, 2005.

[15] L. Lehmann, "Orbital stability," December 2018. [Online]. Available: https://math.stackexchange.com/questions/3042618/stability-vs-orbital-stability-in-odes

[16] U. Mettin, P. La Hera, L. Freidovich, A. Shiriaev, and J. Helbo, "Motion Planning for Humanoid Robots Based on Virtual Constraints Extracted from Recorded Human Motions," Intelligence Service Robotics **1**(4), 2008, pp. 289–301.

[17] A. LLC, "Guidelines for Choosing Feedback Control in Industrial Applications." [Online]. Available: http://www.apicsllc.com/apics/Misc/ff.html

[18] U. Mettin, P. La Hera, L. Freidovich, and A. Shiriaev, "Parallel Elastic Actuators as a Control Tool for Preplanned Trajectories of Underactuated Mechanical Systems," The International Journal of Robotics Research 2010, 29, 2009, pp. 1186–1198.

[19] F. Lang, "Elderly in Japan are Wearing Exoskeletons to Keep Working Past Retirement Age," December 2019. [Online]. Available: https://interestingengineering.com/elderly-in-japan-are-wearing-exoskeletons-to-keep-working-past-retirement-age

[20] V. Tangermann, "The Elderly in Japan are Using Exoskeletons to Delay Retirement," December 2019. [Online]. Available: http://downloadpmfast.com/robotics/sophia-the-humanoid-robotic-is-coming-to-kenya-cio-east-africa/

[21] "Sophia the humanoid robot is coming to Kenya - CIO East Africa," 2019. [Online]. Available: http://downloadpmfast.com/robotics/sophia-the-humanoid-robotic-is-coming-to-kenya-cio-east-africa/

[22] U. H. K. Robot, "BIOLOID GP," 2020. [Online]. Available: https://unclebobtech.com/bioloid-gp-2/

[23] "NAO robot." [Online]. Available: https://stampdesign.com.au/autism/product/nao-robot/